Check for updates

Harnessing selectivity in chemical sensing *via* supramolecular interactions: from functionalization of nanomaterials to device applications

Rafael Furlan de Oliveira, Verónica Montes-García, [iD] Artur Ciesielski [iD] * and Paolo Samorì [iD] *

Chemical sensing is a strategic field of science and technology ultimately aiming at improving the quality of our lives and the sustainability of our Planet. Sensors bear a direct societal impact on well-being, which includes the quality and composition of the air we breathe, the water we drink, and the food we eat. Pristine low-dimensional materials are widely exploited as highly sensitive elements in chemical sensors, although they suffer from lack of intrinsic selectivity towards specific analytes. Here, we showcase the most recent strategies on the use of (supra)molecular interactions to harness the selectivity of suitably functionalized 0D, 1D, and 2D low-dimensional materials for chemical sensing. We discuss how the design and selection of receptors *via* machine learning and artificial intelligence hold a disruptive potential in chemical sensing, where selectivity is achieved by the design and high-throughput screening of large libraries of molecules exhibiting a set of affinity parameters that dictates the analyte specificity. We also discuss the importance of achieving selectivity along with other relevant characteristics in chemical sensing, such as high sensitivity, response speed, and reversibility, as milestones for true practical applications. Finally, for each distinct class of low-dimensional material, we present the most suitable functionalization strategies for their incorporation into efficient transducers for chemical sensing.

Low-dimensional materials (LDMs) exhibiting a high surface-to-volume ratio are unique scaffolds whose interactions with

Université de Strasbourg and CNRS, ISIS, 8 allée Gaspard Monge, 67000 Strasbourg, France. E-mail: ciesielski@unistra.fr, samori@unistra.fr

Rafael Furlan de Oliveira obtained his MSc and PhD degrees from São Paulo State University (Brazil) working on materials science and biosensors. He was visiting scholar at Bangor University (Wales, UK), Università di Modena & Reggio-Emilia (Italy), and Istituto per lo Studio dei Materiali Nano-strutturati – CNR (Italy). In 2014–2018 he was PostDoc at Brazilian Nanotechnology National Laboratory (LNNano) working on molecular/organic electronics. In 2018–2021 he was PostDoc at the Institut de Science et d'Ingénierie Supramoléculaires – Universitè de Strasbourg (France) working on 2D materials-based devices for (bio)sensing. Rafael is currently Head of Nano and Microfabrication Division at LNNano (Brazil).

Rafael Furlan de Oliveira

Verónica Montes-García obtained her PhD degree from the University of Vigo (Spain) under the supervision of Dr Isabel Pastoriza-Santos and Dr Jorge Pérez-Juste. Currently, she is working as a postdoctoral researcher in the group of Prof. Paolo Samorì in the Institut de Science et d'Ingénierie Supramoléculaires (I.S.I.S.). Her research is focused on the synthesis and characterization of new hybrid materials based on metal nanoparticles for the fabrication of optical and electrical chemical sensors.

Verónica Montes-García

the environment drive their application as sensitive elements in chemical sensing.[1–8] They allow prompt reconfiguration of the architectures of the sensor, whose response to the detection of the chosen analyte becomes no longer limited by extrinsic factors such as the slow diffusion of target molecules through the active material or the presence of structural traps for small molecules/ions. The unique features of LDMs determine the highest responsiveness, sensitivity, and reversibility combined with the lowest limit of detection (LoD) in the sensing process. With the advancement of nanoscience and nanotechnology, a large arsenal of LDMs has become available. In particular, 0D – nanoparticles (NPs), 1D – nanotubes (NTs), nanowires (NWs), and nanofibers, as well as 2D – metal–/covalent–organic frameworks, graphene, and related materials represent the ideal sensory components to be readily integrated into devices.[4,9–13] The interaction between LDMs and analytes should preferably occur at the non-covalent level.[14] LDM-analyte covalent binding should be avoided as it leads to irreversible interactions, being suitable only for single-use disposable sensors.[15,16] In fact, non-covalent interactions are sought-after since quick responses and fast recovery rates are required to enable continuous analyte monitoring. However, the main shortcoming is the lack of selectivity of several LDMs towards the analyte, since the interaction between the two components is intrinsically unspecific. Fortunately, such a limitation can be chemically overcome; fine selectivity can be attained *via* functionalization of LDMs with appropriate (supra)molecular receptors which can recognize the target species *via* one or multiple non-covalent interactions (*e.g.*, hydrogen-bonding, metal–ligand bonding, van der Waals, and electrostatic interactions, or hydrophobic forces).[2,14,17] *Ad hoc* chemical receptors should be designed having an optimized size, geometry, dipole and quadrupole moments, and surface charges, ultimately guaranteeing the highest discrimination among chemical species in the sensing process (Fig. 1). In such a way, the detection of ions, heavy metals, small (bio)molecules, and all kinds of analytes can be accomplished with high selectivity and sensitivity by monitoring variations of optical properties (*e.g.*, a change in absorbance and/or fluorescence intensity or Raman signals) or electrical characteristics (*e.g.*, capacitance, resistance, voltage, *etc.*) of LDMs incorporated in suitable transducers. By taking advantage of the major and recent progress in optoelectronics, functionalized-LDMs can be integrated into portable, flexible, lightweight, and low-cost devices operating with ultra-low power for a new generation of sensing technologies, which can be ultimately wearable.[18]

Here, we review the design and fabrication of selective chemical sensors based on functionalized LDMs from the choice of the analyte of interest to the LDM integration into suitable transducers. We discuss the importance of the receptor design and then present the most enlightening and recent strategies developed for the functionalization of LDMs to achieve selectivity *via* (supra)molecular interactions. We also discuss the future directions, challenges, and opportunities to expand the frontiers of chemical sensing towards sensory technologies with potential impact in environmental sciences and biomedical applications. Topics out of the scope of this review include LDM fabrication methods, indiscriminate combinations of several LDMs in a single device to achieve selectivity, and the use of bioreceptors (*i.e.*, biosensors). Our goal is to discuss the major benefits, progress, and limitations derived from the rational and direct functionalization of LDMs with (supra)molecular receptors for selective chemical sensing and practical applications.

Indispensable characteristics and key performance indicators (KPIs) in chemical sensors

Selectivity is the ability of a sensor to exclusively detect the analyte of interest in the presence of other species. This is not a simple task given the enormous number ($>10^7$) of known

Artur Ciesielski obtained his MSc degree from Adam Mickiewicz University, followed by his PhD degree from the University of Strasbourg. In 2016, he became a research associate at the Institut de Science et d'Ingénierie Supramoléculaires (ISIS) and CNRS. In 2018, he was appointed as visiting professor at the Centre for Advanced Technologies of Adam Mickiewicz University in Poznań (Poland). He is member of the Young Academy of Europe (YAE).

Artur Ciesielski

His research interests include the design of supramolecular systems, self-assembly of nanopatterns, and production and chemical modification of 2D materials.

Paolo Samorì is Distinguished Professor at the University of Strasbourg and Director of the Institut de Science et d'Ingénierie Supramoléculaires. He is Fellow of the Royal Society of Chemistry (FRSC), Fellow of the European Academy of Sciences (EURASC), Member of the Academia Europaea, Foreign Member of the Royal Flemish Academy of Belgium for Science and the Arts (KVAB) and Senior Member of the Institut Universitaire de France (IUF). His

Paolo Samorì

research interests comprise nanochemistry, supramolecular sciences, materials chemistry with specific focus on graphene and other 2D materials, functional organic/polymeric and hybrid nanomaterials for application in optoelectronics, energy and sensing.
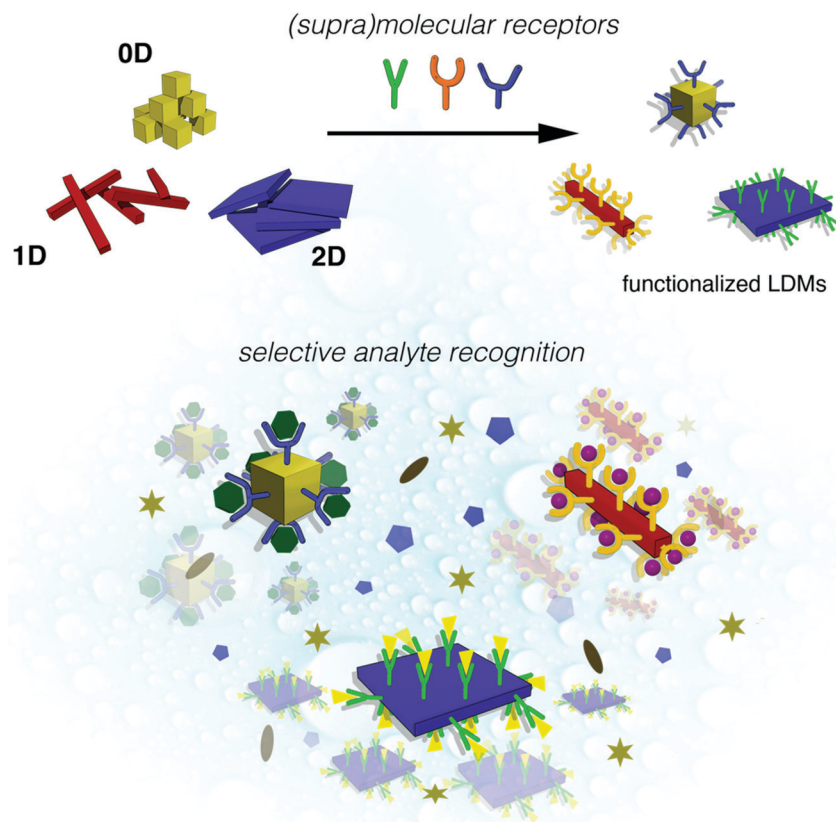
Fig. 1 Representative functionalization of 0D, 1D, and 2D LDMs with *ad hoc* chemical receptors for the (supra)molecular recognition of analyte species in the presence of interfering compounds.

molecular substances and possible chemical similarities between them in terms of size, surface charges, or structure, and their presence in complex media. To ensure efficient selectivity, the receptors targeting the chosen analyte should be optimally immobilized on the LDM's surface either *via* covalent or non-covalent bonds. Such functionalization can be performed either in solution, *i.e.*, before the LDM incorporation into the sensing unit, or directly on the sensor surface. The weak magnitude of (supra)molecular interactions can be inappropriate for the immobilization of receptors on the LDM surface when sensors need to endure long assays or tests in harsh conditions (*e.g.* in saline or acidic/alkaline solutions, or in biological media).[19] In such cases, the use of stronger or multivalent (supra)molecular interactions or even better covalent approaches is more suitable.

While LDM functionalization can be achieved by both covalent and non-covalent strategies, analyte recognition is best regulated by non-covalent interactions. Receptors capable of interacting with analyte molecules *via* (supra)molecular forces include molecular containers, multidentate ligands, polymer coronae, among many other types of molecules and macromolecules.[2,20,21] The arrangement of receptors and the intrinsic properties of LDMs (*e.g.*, the presence of defects or charges) are critical for the sensing properties if not accurately controlled.[22] While selectivity is key, it becomes meaningless

without the cross-reactivity analysis, where the sensor is exposed to a variety of species chemically similar to the target analyte. Several reports claim unprecedented analyte selectivity for a multitude of LDM-based sensors, but the lack of cross-reactivity information makes them irrelevant for real applications.[1] Sensors claimed to be selective without presenting well-grounded cross-selectivity assays are disregarded in this review as they do not hold potential for realistic applications.

Once selectivity is achieved, the LoD and Sensitivity become the most important indicators of the sensor performance. A sensor is considered highly sensitive when it boasts a low LoD, with LoD and sensitivity being frequently regarded erroneously as synonymous. However, while LoD represents the limit below which the detection of an analyte is impossible due to the background noise, sensitivity indicates the capability of the sensor to differentiate between two very close concentrations of the analyte. Alongside, the use of experimental and calculated LoD has also been frequently controversial. As a common example, a sensor calibration curve that can be linearly fitted follows the equation:

$$S = mC + i \qquad (1)$$

where S is the output signal (*e.g.*, absorbance, Raman intensity, electric current, *etc.*), i, the intercept, is known as

noise or error term, m is the sensor sensitivity, and C is the analyte concentration.

The LoD can be calculated from eqn (1), as stated by IUPAC:[23]

$$S_L = S_B + k\sigma_B \qquad (2)$$

where S_L is the smallest detectable signal, S_B is the average input signal, σ_B is the standard deviation of a blank sample (no analyte), and k is a numerical factor chosen following the confidence level desired (usually 3). The LoD is a function of S_L and therefore:

$$LoD = \frac{S_L - S_B}{m} \qquad (3)$$

Because the mean blank reading S_B is not always 0, the signal must be background corrected. Hence:

$$LoD = \frac{k\sigma_B}{m} \qquad (4)$$

However, the LoD value obtained only reflects the real limit of detection when m is well-defined and it is essentially 0. Although this calculated value represents the real limit of the sensor, it is commonly presented as the LoD of the system and the experimental value is never determined or is much higher in absolute terms.

The Responsiveness of a sensor, *i.e.*, the response and recovery time of the output signal, is also of paramount importance. Ideally, most sensors should respond "instantaneously" (<1 s) to the analyte presence. Non-covalent analyte recognition endows fast responses and signal recovery to sensors, being pivotal for continuous monitoring. However, the response and recovery time will depend on the affinity of the receptor for the analyte of interest. The higher is the affinity of the receptor to the analyte, the faster would be detection, but also very likely the slower will be the signal recovery. Therefore, a compromise is required while developing the sensor.

Disposable sensors, *i.e.*, single-use devices (*e.g.*, paper strips for pregnancy tests or personal glucose meters), do not suffer from such a trade-off, as sensor recovery is not necessary.

Analytes and their (supra)molecular receptors

To implement selectivity in chemical sensors, the careful choice or design of an *ad hoc* receptor is of utmost importance. While receptors that display proven selectivity towards a given analyte can be used to develop a new type of transducer or technology, uncommon or unexplored analytes will demand the design and synthesis of novel artificial receptors with optimized affinity. Thus, the first step to program selectivity in chemical sensing is to have a clear understanding of the chemical constitution of the target analyte and possible existing interfering compounds.[24] Analytes of interest are manifold and can be roughly classified as cations and anions, gases, biologically-relevant molecules, explosives, toxic substances (*e.g.*, polycyclic aromatic hydrocarbons (PAHs), pesticides, environmental pollutants, *etc.*), pharmaceutical agents, to name a few.[4,8,9,11,17] The greater the structural and chemical complexity of the analyte (*e.g.*, large molecules with numerous and different chemical groups), the more challenging is the receptor design. For instance, to ensure the selective detection of metal cations (a class of relatively simple analytes), their size (ionic or hydrated radius), charge density, and 'hardness' are the important characteristics to be considered. Even if such aspects to be considered are narrow and the underlying principles for the metal complexation are relatively well understood, the number and variety of receptors for metal cations that can be found in the literature are vast (see Fig. 2). To illustrate that, let us consider the detection of heavy metal ions (HMIs), which are an environmental threat with severe consequences to human health. According to the European Parliament and the Council of the European Union,[25] some
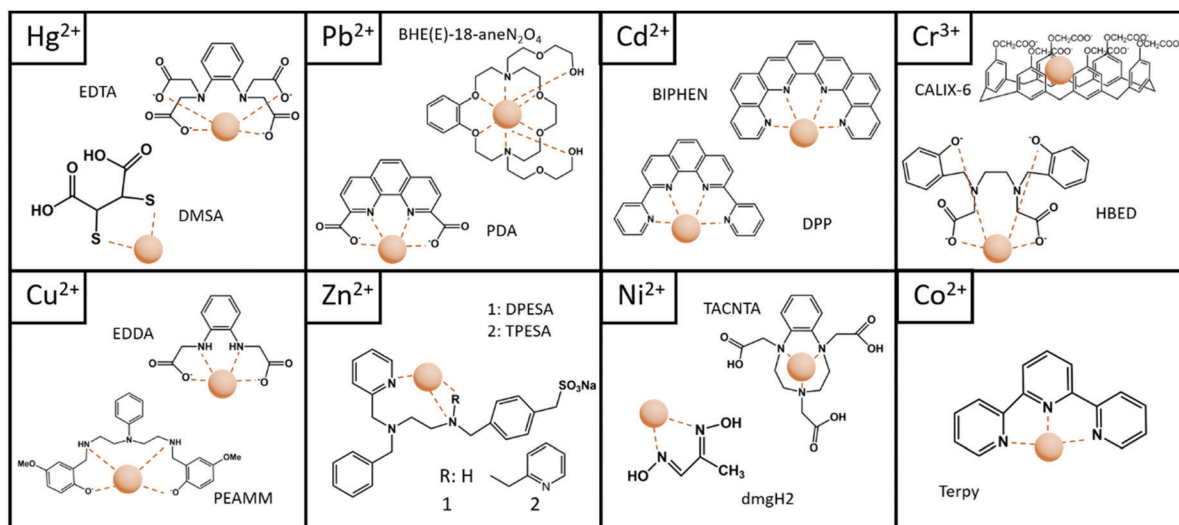

Fig. 2 Schematic representation of some (supra)molecular receptors for HMIs (illustrated as a brown sphere) and their binding sites.

hazardous HMIs and their maximum allowed content in drinkable water for safe consumption are: Hg^{2+} 1 ppb; Pb^{2+} 5 ppb; Cd^{2+} 5 ppb; Cr^{3+} 50 ppb; Cu^{2+} 2 ppb; Zn^{2+} not yet regulated; Ni^{2+} 20 ppb and Co^{2+}. By screening the literature, a wide range of multidentate ligands presenting high affinity towards such HMIs for use as (supra)molecular receptors can be found (Fig. 2). These include ethylenediaminetetraacetic acid (EDTA)[26,27] and *meso*-2,3-dimercaptosuccinic acid (DMSA)[28,29] derivatives for Hg^{2+}, 1,10-bis(2-(2-hydroxyethoxy)ethyl)-4,7,13,16-tetraoxa-1,10-diazacyclooctadecane (BHE(E)-18-aneN_2O_4)[30] and 1,10-phenanthroline-2,9-dicarboxylic acid (PDA)[31] for Pb^{2+}; 2,2′-bi-1,10-phenanthroline (BIPHEN)[32] and (2,9-di-(pyrid-2-yl)-1,10-phenanthroline) (DPP)[33] for Cd^{2+}; calix[6]arene (CALIX-6)[30] and *N*,*N*/-bis(2-hydroxybenzyl) ethylenedi-amine-*N*,*N*-diaceticacid (HBED)[30] for Cr^{3+}; ethylenediamine-*N*,*N*′-diacetic acid (EDDA)[34] and 2,2′-((((phenylazanediyl) bis(ethane-2,1-diyl))bis(azanediyl))bis(methylene))bis(4-methoxyphenol) (PEAMM)[35] for Cu^{2+}; (4-{[2-(bis-pyridin-2-ylmethylamino)ethylamino]-methyl}phenyl)methanesulfonic acid, sodium salt (DPESA)[36] and [4-({[2-(bis-pyridin-2-ylmethylamino)ethyl] pyridin-2-ylmethylamino}-methyl)phenyl]methanesulfonic acid, sodium salt (TPESA)[36] for Zn^{2+}; 1,4,7-triazacyclononane-*N*′,*N*′,*N*″-triaceticacid (TACNTA)[30] and dimethylglyoxime (dmgH2)[37] for Ni^{2+}; and various terpyridine (terpy) derivatives[38,39] for Co^{2+} recognition.

It is fair to note that a definitive receptor for a given HMI does not exist. Similarly, if we consider the recognition of spherical anions, such as Cl^- or Br^-, the design and selection of receptors would follow pretty much the same guidelines as those discussed for metal cations. Again, a vast repertoire of chemical ligands for simple anions can be found.[20,21,40] Upon increasing the structural complexity of the target analyte, the design of an efficient receptor becomes more and more sophisticated. For example, for non-spherical ionic species, additional aspects such as hydrogen bond donor/acceptor characteristics should be considered. Charged organic analytes may require receptors with both hydrophilic and hydrophobic regions, while neutral species may lack specific 'handles' such as polar groups that can strongly interact with the receptor. Since receptor-analyte interactions occur through binding sites, the number of such receptor binding sites must be selected in a fashion that is most complementary to the characteristics of the target analyte, but not with those of the interfering compounds. Affinity, which is a function of receptor binding size, the ease of access to its binding pocket, cavity, or cleft by the target molecule, and association *via* multiple (supra)molecular interactions, are described by a set of thermodynamic and kinetics parameters. These are translated into the binding (or association) constant, which can be recalculated as the free energy of binding, binding enthalpy and/or entropy, kinetic adsorption and desorption constants, and activation energies for binding and dissociation.[20]

Extensive knowledge (especially quantitative information) on such affinity-related parameters is pivotal for the appropriate choice or design of a receptor. Such information can be obtained both from experimentation and simulation.

Experimental affinity data include assays in solution *via* titration and analysis of the receptor-analyte binding by a multitude of analytical methods, studies in the condensed phase from Langmuir isotherms, and on surface from electrochemical, mechano-acoustical (*e.g.*, quartz crystal microbalance), or optical techniques (*e.g.*, surface plasmon resonance, SPR). Computational approaches include hybrid quantum mechanics/ molecular mechanics simulations and density functional theory (DFT) studies. Over the years, the amount of data has become immensely large, so the design and selection of artificial receptors do not need to rely solely on the human ability to read the literature to select the best examples or to implement novel synthetic strategies. Machine learning and artificial intelligent tools have boomed recently for predicting properties of materials and their rational design.[41] However, to the best of our knowledge, the use of machine-learning methods for selecting or designing appropriate chemical receptors has yet not been fully achieved. Most machine-learning approaches for sensing focus on pattern recognition of multidimensional multisensor response (*e.g.*, e-tongues) to discriminate analytes from their interfering species.[42] In this case, selectivity is achieved *via* some sort of serendipity instead of being a foreseen or programmed event. Fortunately, some initial attempts to identify how different chemical receptor groups interact with the target analyte using machine-learning become to flourish in the literature.[43]

The *in silico* determination of (supra)molecular receptors *via* machine-learning would involve building up a framework based on a set of affinity parameters, such as the binding/ association constants and related quantities for several known receptor-analyte pairs (*e.g.*, metal–ligands).[44] Such descriptive parameters should be broad, *e.g.*, by using their minimum, mean, and maximum values, range, and mean absolute deviation, found in the literature under varied conditions (*e.g.*, temperature, solvent medium, *etc.*) to ensure flexibility for the model processing. Yet, they need to be specific enough to guarantee that the set of affinity parameters has a unique correspondence with the target analyte. The input can be either experimental or computational (*e.g.*, DFT calculations) data. It is not necessary to know exactly how each characteristic of the receptors (*viz.*, their chemical groups and properties) affects the selectivity for the analyte. This information is already accounted into such affinity parameters, and the receptor-analyte relationships will arise from the machine-learning processing.[41] The next step is to train the models with a large data set of selected attributes using a few supervised available algorithms. Several already-developed, multi-purpose machine-learning algorithms are available (*e.g.*, Random Forest, k-Nearest Neighbours, Support Vector Machines, Adaptive Boosting, Artificial Neural Networks, *etc.*), each of them presenting unique advantages.[45] The method must be agnostic to the type of training, thus using multiple algorithms is recommended for improved accuracy. Data partitioning, *i.e.*, grouping the data set into chemically similar parts and training a different model on each subset, increases the predictive power of the models under evaluation.[41,46] Following, the model must

be validated and tested against several known receptor-analyte affinity attributes. Finally, high-throughput calculations will allow to one screen larger amounts of chemical structures (*viz.* millions of molecules) as potential receptors for the target analyte specie.[41,44] Thus, any compound envisaged as *ad hoc* chemical receptor (existing or idealized) can be verified against the model to predict its affinity towards the analyte prior to any synthetic development or LDM functionalization. Chaube *et al.*,[44] for example, developed a machine learning framework for predicting binding affinities of lanthanide cations with several structurally diverse molecular ligands. They employed 698 organic and inorganic ligands, 15 lanthanide cations, and 8 solvent media in the model, which was then used to screen 71 million molecules from a public repository. The determined binding affinities for several cation–ligand pairs were compared with the experimental values from the literature, which is the basis for choosing the best ligand(s) for a given (or set of) lanthanide cation(s). However, no functionalization of LDMs with such selected potential receptors or a practical chemical sensor have been demonstrated, which emphasizes the need for strengthening the relationships between experimental research and data science.

The predictive design of artificial receptors *via* machine learning holds a disruptive potential in chemical sensing and perhaps can one day mimic the intrinsic high affinity of bioreceptors, such as enzymes and antibodies, where several (supra)molecular interactions orchestrated by nature ensure fine selectivity. Various review articles discuss the characteristics of a multitude of existing (supra)molecular receptors and the assessment of their specificity for the detection of metal cations,[47] anions,[47,48] gases,[47] PAHs,[47,49] explosives,[47,50] and pesticides.[47,51] Covering such a wide variety of receptors would need an extensive review, which is out the scope here. Readers can find more about the synthetic receptors for chemical sensing by referring to books dedicated to this topic.[20,21]

Functionalization of LDMs with chemical receptors

Once the *ad hoc* receptor for the analyte of interest is defined, the next step consists of its anchoring on the LDM surface. The density and arrangement of receptors on the surface need to be optimized to avoid uncoated areas (source of unspecific analyte binding), so that all available recognition sites interact simultaneously with the analyte. The most stable complexes are generally obtained with receptors that are pre-organised (*i.e.*, covalently anchored on LDM surface) for analyte binding, where there is no entropically and enthalpically unfavourable rearrangement on binding that reduces the overall free energy of complexation. In the following, we present the LDMs frequently employed in chemical sensing and a summary of their main functionalization routes.

0D Nanostructures

0D structures or NPs have been exploited in chemical sensors for decades because of their high chemical stability, high surface-to-volume ratio, and unique optoelectronic properties resulting from the space confinement. NPs, which include metals, metal chalcogenides, oxides, and quantum dots can be produced at high yield with full control over their size, structure, and composition through straightforward colloidal chemistry.[4,52] Typically, the synthetic routes presently exploited to fabricate functionalized NPs are: (i) receptor-mediated reduction and stabilization, (ii) seeded growth combined with receptor stabilization, and (iii) NP post-synthetic modification.[53–55] Post-synthetic NP functionalization, *i.e.* ligand exchange reaction or secondary modification, is the most versatile for sensing, which allows the use of countless molecular receptors, opening numerous options for ensuring analyte selectivity.[53] Independently of the synthetic route, the most extensively employed NP functionalization strategy relies on metal–thiol covalent linkage. In fact, various receptors having thiol or other sulfur-containing moieties can covalently tether metallic and metal oxide surfaces.[56,57] More harsh approaches towards these linkages include metal–carbon (by aryl diazonium derivatives),[58] metal–carbene or metal–nitrene (*via* diazo derivatives),[59] or metal–acetylide/–vinylidene (*via* acetylene derivatives)[60] covalent bonds. Despite its weaker interactions, amines, ammonium ions, negatively charged carboxylate groups and phosphines can also be used for the effective NP functionalization.[53,61]

1D Nanostructures

1D nanostructures are high aspect ratio LDMs, typically classified as NWs, NTs, nanofibers, nanobelts, nanofilaments, and nanoribbons. Metal, metal oxide, inorganic and polymer semiconductor NWs, and carbon NTs (single or multiwalled) are some of the main 1D LDMs exploited for chemical sensing.[9,62] Each 1D nanostructure can also exhibit a multitude of distinct characteristics depending on their composition and structure, *e.g.* single or compound semiconductor NWs, carbon NTs (CNTs) of different chirality and electrical properties (metallic or semiconducting), *etc.*, leading to unlimited possibilities for the rational design of chemical sensors. For CNTs, non-covalent functionalization often involves their physical mixing with small molecules or macromolecular receptors, where tethering is driven by van der Waals forces, hydrophobic, or π–π interactions.[9] CNT covalent modification, on the other hand, can be achieved by side-wall reactions or at the CNT termini *via* a variety of methods by exploiting intrinsic or induced defects.[63] A common covalent strategy to functionalize the end-tip of CNTs relies on their oxidation to produce carboxylic acid moieties, which are further used to graft specific receptors *via* amidation/esterification linkage or carboxylate–ammonium interactions.[62] Both non-covalent sidewall functionalization or end-tip covalent modification of CNTs are preferred to minimally perturb their π-delocalized electronic system and related electrical and optical properties (*e.g.* conductivity, bandgap, *etc.*). Yet, covalent approaches require careful control to achieve an optimal balance between the degree of functionalization and preservation of the CNT

π-delocalized electronic system. Regarding conducting polymer (CP) 1D structures, their functionalization can also be achieved by non-covalent approaches, such as physical mixing, or covalent modifications based on side-chain reactions, copolymer formation, and molecular grafting, depending on the CP chemical composition.[62] Metal and metal oxide NWs can be functionalized with molecules bearing a thiol, amine, silane, or phosphonic acid anchoring moiety to introduce functional groups for further grafting of *ad hoc* receptors, similarly to the functionalization strategies discussed for 0D nanostructures.

2D Nanostructures

2D materials (2DMs) equally possess great potential for chemical sensing resulting from their distinct properties determined by their atomically thin structure.[10,11,64–67] Their lightweight and highest surface-to-volume ratio make them particularly suitable for coating large surfaces. Graphene, transition metal dichalcogenides (TMDs), metal oxides, nitrides, and carbides, along with single-element graphene analogues known as MXenes, compose a plethora of chemically and structurally distinct 2DMs with vastly diverse properties.[10,11,64,67] For example, graphene's elevated charge carrier mobility ($> 10\,000$ cm^2 V^{-1} s^{-1}) is very appealing for sensors with an electrical readout, while the TMD tuneable band structure is a powerful resource to develop optical sensors.[65,66] Depending on the production method, the degree of defectivity in 2DMs varies significantly thereby impacting their properties, processability, and ultimately the sensor performance.

The decoration of 2DMs with selective *ad hoc* receptors can be achieved *via* diverse methods, depending on the 2DM of choice and receptor.[68–70] For example, graphene oxide (GO) and reduced graphene oxide (rGO) are graphene-based materials whose processability complies with industrial fabrication requirements (*e.g.*, large-scale solution processing and coating methods)[71] and the abundancy of oxygen-groups are ideal for functionalization *via* covalent binding. Such excess of oxygen groups makes the GO's surface highly negatively charged, which is an additional advantage for its functionalization *via* electrostatic interactions. Among the most common strategies is the functionalization of GO and rGO with macrocyclic host molecules (*viz.* cyclodextrins,[72,73] calixarenes,[74,75] pillararenes,[76] crown ethers,[77] cucurbiturils,[78] *etc.*) which is known to yield stable host–guest complexes with several organic, inorganic, biological guest analyte molecules via (supra)molecular interactions. The functionalization is typically achieved *via* the so-called wet-chemical method where GO is dispersed in solution in the presence of the macrocyclic receptor, followed or not by its chemical reduction depending on the sensing technology. The receptor molecule binds non-covalently to the large surface area of GO (or rGO) flakes at high loads, for example, larger than on CNTs (*ca.* 38.2 wt% *vs.* 9.5 wt%).[79] While the key role played by the oxygen-containing groups in GO and rGO is perfectly highlighted by their functional capabilities, those groups cannot be fully eliminated during the material functionalization. Such remaining oxygen groups on the basal plane and at the edges of 2D sheets jeopardize the material's selectivity, as they bring into play spurious background dipolar interactions which cannot be easily distinguished from the desired receptor-analyte signal.

Graphene – the first reported and most studied 2DM – has been extensively employed in chemical sensing mainly thanks to its remarkable electrical properties. In particular, graphene's extended sp^2-hybridized carbon network makes it especially suitable for functionalization with planar aromatic molecules *via* π–π stacking.[69,70,80] Pyrene-derivatives bearing a functional substituent or receptor moiety can functionalize graphene without disrupting its extended honeycomb structure and resulting outstanding electronic properties. The majority of applications though that use of pyrene-derivatives to functionalize graphene still relies on the immobilization of bioreceptors for biosensing.[81–83] Alternatively, covalent methods to functionalize graphene can be achieved *via* the activation of point defects (*i.e.* absent sp^2 carbon atoms on the basal plane) using highly reactive free radicals, such as those produced by diazonium salts or benzoyl peroxide.[84,85] This process, however, if carried out in excess can jeopardize the remarkable electrical properties of graphene. Finally, non-graphene 2DMs for sensing include mostly semiconducting TMDs, black phosphorous (BP)/phosphorene, and MXenes. While numerous applications rely on non-functionalized 2D materials[11,66,86,87] examples employing *ad hoc* chemical receptors for selective recognition are very scarce (see Table 1), indicating a window of opportunity for materials and strategies of this kind. A few examples of functionalized non-graphene 2DMs include the non-covalent wet-chemical strategy of BP sheets with macrocyclic receptors[88] and the covalent attachment of thiol-modified molecules at the sulphur vacancies of MoS_2.[89] The rational exploration of natural or induced defects in 2DMs for attaining new functionalities is a powerful strategy for sensing.

LDM integration into sensing platforms

LDMs can be produced *via* either top-down (*e.g.*, lithography, focused ion beam milling, *etc.*) or bottom-up approaches (*e.g.*, chemical or electrochemical deposition, self-assembly, *etc.*). The incorporation of LDMs of different size (diameter, length-to-diameter ratio, or lateral size), chemical composition (mono- or multi-elemental structures, such as core–shell), structural complexity (individual LDMs or arrays thereof), and arrangement (aligned or unaligned distribution, with varying density) into sensing platforms can be achieved by two major strategies: (i) *in situ* growth of the LDMs right onto a device platform (*e.g.*, paper strips, pre-patterned electrodes, *etc.*), or (ii) *ex situ* growth of the LDMs, followed by their transfer to the transducer's surface. *In situ* growth of LDMs on a device platform usually leads to more robust and industrially compatible approaches. Meanwhile, *ex situ* growth and manipulation of LDMs take great advantage of the major steps forward made by

Table 1 LDMs-based systems for selective chemical sensing and their respective KPIs

Analyte	Receptor	LDM	Sensing strategy	Tested interfering compounds	LoD	Working range	Response time	Ref.
Cations								
As^{3+} and As^{5+}	Dimercaptosuccinic acid	Au NPs	Colorimetric	Na^+, K^+, Cd^{2+}, Cr^{3+}, Fe^{3+}, Pb^{2+}, Cu^{2+}, Ca^{2+}, Hg^{2+}, Mg^{2+}, Ni^{2+}, NO_3^-, and F^-	1 ppb (naked eye)	0.001–10 ppm	—	91
Cu^{2+}	Formaldehyde modified hyperbranched polyethyleneimine	Au NPs	Fluorescence	Na^+, K^+, Cl^-, Br^-, I^-, PO_4^{3-}, HPO_4^{2-}, $H_2PO_4^{1-}$, SO_4^{2-}, NO_3^-, Mg^{2+}, Mn^{2+}, Zn^{2+}, Cd^{2+}, $S_2O_3^{2-}$, SO_3^{2-}, HSO_3^-, H_2O_2, Ca^{2+}, Pb^{2+}, Al^{3+}, Fe^{3+}, Hg^{2+}, Ni^{2+}, Ba^{2+}, Co^{2+}, Cr^{3+}, Fe^{2+}, S^{2-} and CrO_4^{2-}	77 nM	0.15–23 μM	2 min	92
	N-[4-Methylthiobenzyl]-N,N-bis(2-pyridylmethyl)amine	Au NPs	SERS	Co^{2+}, Zn^{2+}, Mn^{2+}, Ni^{2+}, Fe^{3+} and Fe^{2+}	3.5×10^{-8} M	5×10^{-8}–5×10^{-6}	2 min	93
	N-(2-(1-(p-Tolyl)-1hphenanthro[9,10-d]imidazol-2-yl)phenyl)picolinamide	rGO	Electrochemical	Na^+, K^+, Mg^{2+}, Al^{3+}, Pb^{2+}, Cd^{2+}, Co^{2+}, Fe^{2+}, Zn^{2+}, Ni^{2+}, Hg^{2+}, SO_4^{2-}, Cl^-, PO_4^{3-}	0.67 μg L^{-1}	5–300 μg L^{-1}	>360 s	94
Hg^{2+}	Thiacalix[4]arene	Graphene	TFT	Na^+, Mg^{2+}, Ni^{2+}, and Cd^{2+}	1 μM	1 μM–1 mM	15 min	74
	4-Mercaptopyridine	Au NPs	SPR	Fe^{2+}, Cu^{2+}, K^+, Na^+, Pb^{2+}, Ni^{2+}, Ba^{2+}, Ca^{2+}, Zn^{2+}, and Fe^{3+}	8 nM	0.008–30 μM	15 min	95
	Histidine conjugated perylene diimide bola-amphiphile	Au NPs	SERS	Na^+, K^+, Li^+, Cu^{2+}, Cd^{2+}, Co^{2+}, Fe^{3+}, Mg^{2+}, Pb^{2+}, Ca^{2+}, Zn^{2+}, Ni^{2+}, Cr^{3+}, Ag^+, Al^{3+}, and Fe^{2+}	60 aM	1 fM–1 μM	30 min	96
Pb^{2+}	β-Cyclodextrin	MWCNTs	Electrochemical	Cd^{2+}, Cu^{2+}, Hg^{2+}, Zn^{2+}, and Ni^{2+}	0.9 ppb	3.1–103.3 ppb	—	97
Fe^{3+}, Cd^{2+}, Pb^{2+} (simultaneously)	Calixarene	rGO	Electrochemical	Zn^{2+}, Mg^{2+}, Mn^{2+}	0.02 nM	0.1 nM–0.01 μM	25 min	75
K^+	Dithiomethylene dibenzo-18-crown-6 ether	Au NPs	Chemiresistor	Na^+, Ca^{2+} and Mg^{2+}	1 μM	1–1000 μM	18 s	98
Anions								
NO_2^-	Poly(acrylamide-co-2-hydroxyethyl acrylate-co-N0-vinyl carbazole) (PAHN)	MWCNTs	Electrochemical	NO_3^-, $FeCl_3$, sodium citrate, urea, glucose	0.003 μM	0.01–25 μM	>50 s	99
NO_3^-	Benzyltriethylammonium chloride	rGO	TFT	Cl^-, SO_4^{2-}, CO_3^{2-}	1.1 μg L^{-1}	0.0028–28 mg L^{-1}	2–7 s	100
AcO^-	3,5-Bis(trifluoromethyl)phenyl squaramide	SWCNTs	Chemiresistor	Cl^-, Br^-, and NO_3^-	0.17 mM	0.17–83.33 mM	>3 min	101
Gases								
NO	Iron phthalocyanine	N-Doped graphene	Electrochemical	K^+, Cl^-, Na^+, Ca^{2+}, SO_4^{2-}, NO_2^-, glucose, NO_3^-	180 nM	0.18 μM–0.4 mM	<4 s	102
	Meso-tetra(4-carboxyphenyl)porphyrin	rGO	TFT	Uric acid, sodium ascorbate, glycine, L-arginine, H_2O_2, and KNO_3	1 pM	1 pM–100 nM	480 ms	103
Biologically relevant molecules								
Norepinephrine	Benzaldehyde and boronic acid	Au NPs	Colorimetric	Dopamine, epinephrine, 5-hydroxyindoleacetic acid, L-tyrosine, glucose, uric acid, lysine, and glutamic acid	0.07 μM	0.1–1 μM	5 min	104
Dopamine	β-Cyclodextrin	Au NPs	Fluorescence	Riboflavin, pyridoxal-5-phosphate, lipoic acid, homovanillicacid, vanillyl mandelic acid, glucose, lactose, cysteine, glycine, tryptophan, valine, arginine, phenylalanine, L-proline, allantoin, the oxidized and reduced form of glutathione, cholesterol, creatinine, homocysteine thiolactone, melamine, H_2O_2, uric acid, and ascorbic acid	20 nM	100.0 nM–80.0 μM	10 min	105

Table 1 (continued)

Analyte	Receptor	LDM	Sensing strategy	Tested interfering compounds	LoD	Working range	Response time	Ref.
Albumin	Carboxylate-functionalized polycarbodiimide polymer	SWCNTs	Fluorescence	Transferrin, and γ-globulin	3 mg L^{-1}	3–100 mg L^{-1}	20 min	106
Insulin	C$_{16}$Polyethylene glycol-ceramide corona	SWCNTs	Fluorescence	Albumin, immunoglobulin G (IgG), fibrinogen, α$_1$-antitrypsin, transferrin, haptoglobin, α$_2$-macroglobulin, IgA, IgM, α$_1$-acid glycoprotein, apolipoprotein A-I, insulin, human chorionic gonadotropin, and C-reactive protein	Not quantified	180 pM–3.5 μM	>30 min	107
Enantiomeric discrimination of 19-aminoacids, and achiral Glycine (Gly)	α,β,γ-Cyclodextrins and cucurbit[n]juril	MoS$_2$	Fluorescence	19 L – and D-amino acids, and Gly	500 μM	20 nM–500 μm (for model L-Tryptophan)	> 30 min	89
Enantiomeric discrimination of tryptophan (Trp)	6-O-α-Maltosyl-β-cyclodextrin	BP	Electrochemical	Tyr, His, Phe, ascorbic acid, glucose, L-Ser, L-Phe, KCl, NaCl, CaCl$_2$, CuCl$_2$, Mg(NO$_3$)$_2$, Al(NO$_3$)$_3$, Zn(NO$_3$)$_2$	1.07 μM (L-Trp) and 1.71 μM (D-Trp)	0.01–1 mM	—	88
	γ-Cyclodextrin	rGO	Electrochemical	D- and L-Alanine, arginine, aspartic acid, cysteine, glutamic acid, glutamine, histidine, leucine, lysine, mandelic acid, methionine, proline, serine, tartaric acid, threonine, valine	54 μM (D-Trp), 21 μM (L-Trp)	100 μM–1 mM	–	72
Toxic substances								
Quinalphos	A complex between Cu^{2+} and tailor-made polymer	Au NPs	Fluorescence	Dichlorvos, profenophos, ethion, triazophos, phorate, phosphemedon, ATP, ADP, AMP, NAD, and NADH	2.4 nM	1–5 μM	3 min	56
Explosives								
2,4,6-Trinitrotoluene (TNT)	p-Aminobenzenethiol	Ag NPs	SERS	Nitrobenzene, 4-nitrotoluene, 2-nitrotoluene, 2,6-dinitrotoluene, and 2,4-dinitrotoluene	0.95 nM	0.001–1.0 μM and 1.0–20.0 μM	200 s	108
	Water-soluble pillar[6]arene	Nitrogen-doped carbon quantum dots	Electrochemical	Nitrobenzene, 4-nitrotoluene, 2-nitrotoluene, 2,6-dinitrotoluene, and 2,4-dinitrotoluene	0.95 nM	0.001–1.0 μM and 1.0–20.0 μM	200 s	108
	Cu-Based metal–organic polyhedra cage	Si NW	TFT	2,4-Dinitrotoluene (2,4-DNT), 4-nitrotoluene (4-NT)	100 pM	1 nM–1 μM	—	109
Pharmaceutical agents								
Kanamycin	4-Amino-3-hydrazino-5-mercapto-1,2,4-triazole	Au NPs	Colorimetric	Tetracycline, L-arginine, L-aspartic acid, glucose, glutathione, glycine, L-lysine, L-phenylalanine, Na$^+$, K$^+$, Mg$_2^{2+}$, and Ca^{2+}	0.004 μM	0.005–0.1 μM; 0.1–20 μM	10 min	110
Acetaminophen and 17β-estradiol	β-Cyclodextrin	MWCNTs	Electrochemical	Na$^+$, K$^+$, Mg^{2+}, Ca$_2^+$, Cl$^-$, SO$_4^{2-}$, glucose, dopamine, ascorbic acid, uric acid, L-serine, L-proline	Acetaminophen (3.3 nM), 17β-estradiol (2.5 nM)	Acetaminophen (0.005–20 μM), 17β-estradiol (0.01–15 μM)	>600 s	111
Acetaminophen	Pillar[5]arene	rGO	Fluorescence	Glucose, sucrose, tween 20, NaCl, KCl, bovine serum albumin, ascorbic acid, uric acid, dopamine, tyrosine, p-nitrophenol, and hydroquinone	0.05 μM	0.1–4.0 μM; 4.0–32 μM		112
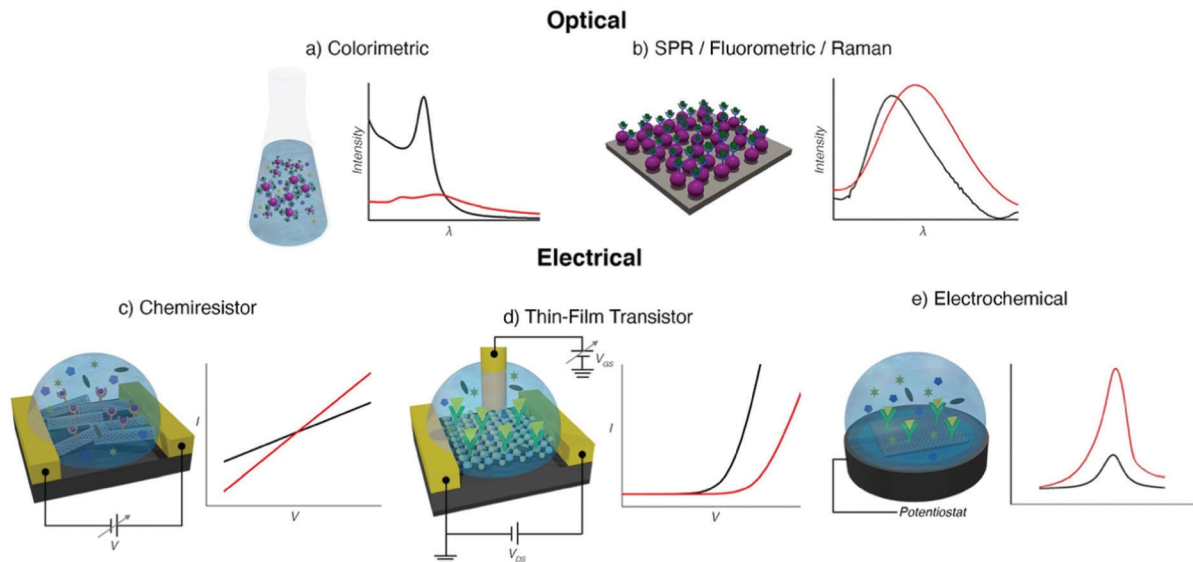
Fig. 3 Archetypical optical (a and b) and electrical (c–e) chemical sensors based on functionalized LDMs with *ad hoc* receptors and (supra)molecular recognition. (a) Colorimetric sensor based on Au NPs. (b) SPR/fluorometric/Raman sensor based on 0D Au NPs deposited on a substrate. (c) Chemiresistor sensor based on carbon nanotubes (CNTs). (d) Thin-film transistor sensor based on MoS_2. (e) Electrochemical sensor based on graphene. In all the assays sensors are exposed to the target analyte of interest and other interfering compounds. Detection of the target analyte can be accomplished by monitoring a variation of optical properties (a and b) (*e.g.* a change in absorbance and/or fluorescence intensity or Raman signals) or a modification of the electrical characteristics (c–e) (*e.g.* capacitance, resistance, or voltage) I denotes electric current, V and E are electrical potentials, and λ is the wavelength. In all cases, the black curves represent the system response in absence of the analyte and the red curves after the sensing events.

nanoscience and nanotechnology over the years. Their incorporation into sensing devices is always challenging, depending on the nature of the materials and interfaces involved and the desired transducing technology. Some top-down methodologies (*e.g.*, lithography, focused ion beam milling) allow for large-scale production of *in situ* grown LDMs and devices thereof with no requirements for material purification, allowing the production of architectures of varied shape, size, and arrangement. Other top-down methodologies, such as exfoliation of 2DMs also guarantee large-scale production of *ex situ* grown LDMs, but the presence of adventitious impurities and the formation of defects may jeopardize the materials' properties and the sensor performance. For bottom-up approaches, the main challenge is to transfer the optimal conditions for the synthesis, purification, and assembly of *in situ* or *ex situ* growth LDMs found in a test tube at a laboratory scale to the device surface at the industrial manufacturing level.

Signal transduction

The most common signal transduction methods employed in LDM-based chemical sensors are optical, electrical, and electrochemical (Fig. 3). Optical transductions are mainly based on changes in absorption, fluorescence, SPR, or Raman signal as a result of the LDM interaction with the analyte (Fig. 3). In particular, colorimetric sensors, both in solution or in paper strips, are ideal for wide use by the general public (*e.g.*, home pregnancy or glucose tests), given their operative simplicity and easiness in the readout, either qualitatively by naked eye reading or (semi-)quantitatively using a smartphone camera.

Electrical and electrochemical sensors, which measure changes in current, electrical potential, or capacitance that result from the interaction between the analyte and LDM-coated electrodes, are suitable for hand-held technologies, exhibiting characteristics such as fast response and elevated accuracy.[90] Common methods to observe such changes include chrono-potentiometry and -amperometry, impedance spectroscopy, current–voltage measurements on both two- and three-terminal devices, such as chemiresistors (CRs) and thin-film transistors (TFTs), respectively (Fig. 3). The integration of LDMs in portable, low-power consumption transducers is an important and challenging step in the technological development of sensors, especially for realizing Point-of-Care (PoC) devices and for fostering the tremendous pace of the Internet of Things (IoT) applied to sensing.

Best performing selective chemical sensors

The most relevant and recent examples of selective chemical sensors functionalized with *ad hoc* (supra)molecular receptors for each family of analytes are reported in Table 1. Representative examples for each LDM type (0D, 1D, and 2D) and transduction technology are described in detail.

Sensors based on 0D LDMs

Depending on the recognition event, the sensor readout can be a change in the optical properties,[56,91–93,95,96,104,105,110,113] or in
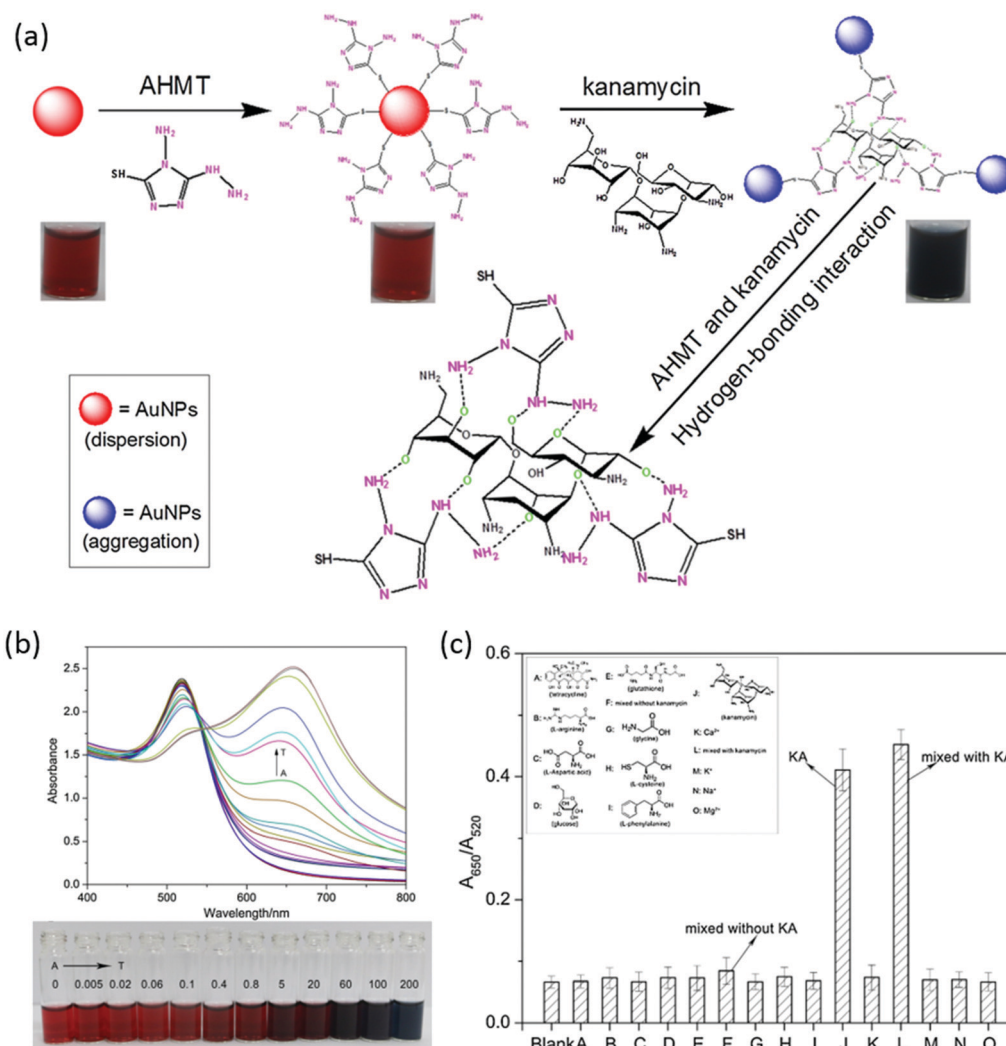
Fig. 4 0D optical sensor based of Au NPs functionalized with using 4-amino-3-hydrazino-5-mercapto-1,2,4-triazole (AHMT) for kanamycin (KA) detection. (a) Colorimetric detection of KA antibiotic using AHMT-functionalized Au NPs based on the hydrogen-bonding interactions. (b) UV-vis absorption spectra (top) and colour changes (bottom) of AHMT–Au NPs in the presence of different KA concentrations at pH 7.4, at room temperature (A to T express the various KA concentrations in μM). (c) The absorption ratio at specific wavelengths (A_{650}/A_{520}) of AHMT–Au NPs *versus* different kinds of similar substances and metal ions (20 μM) at pH 7.4 at room temperature (A to O express the Tetracycline, L-arginine, L-aspartic acid, glucose, glutathione, mixed without KA, Glycine, L-cysteine, L-phenylalanine, kanamycin, Ca^{2+}, mixed with KA, K^+, Na^+, and Mg^{2+}, respectively). The concentration of KA was 5 μM while those of the other chemicals were 20 μM. Error bars were obtained from three experiments. Adapted from ref. 114 with permission of Elsevier.

the electrical characteristics[98,108] of 0D nanostructures. The extraordinary optical properties of metallic NPs due to the plasmonic phenomenon have given rise to the rapid development of colorimetric sensors. In such sensors, the introduction of target analytes or ions can induce the localized SPR shift of the plasmonic NPs functionalized with specific receptors, either in solution or deposited into a solid platform, which is accompanied by a visual colour change.[91,104,110] To illustrate that, we shall consider the work of Qin *et al.* for the detection of kanamycin (KA) antibiotic (Fig. 4) using 4-amino-3-hydrazino-5-mercapto-1,2,4-triazole (AHMT) functionalized Au NPs.[114] AHMT ligand was chosen because it possesses a mercapto group that chemisorbs onto the surface of Au NPs and also bears amino head groups that can interact with KA *via*

hydrogen-bonding. Hence, when Au NPs functionalized with AHMT are exposed to KA solution, the latter coordinates with three AHMT ligands triggering the Au NPs aggregation (Fig. 4a). As a result, the colour of the AHMT–Au NPs solution changed from wine red to deep purple with the increasing concentration of KA (Fig. 4b). Taking advantage of the hydrogen-bonding nature of the (supra)molecular recognition, KA was quantitatively detected in two linear ranges: 0.005–0.1 μM and 0.1–20 μM, with a LoD as low as 0.004 μM. Furthermore, the authors tested the cross-selectivity of the sensor by exposing it to different interfering chemicals, including common amine acid, antibiotics, and metal ions, demonstrating a remarkable selectivity (Fig. 4c).

In addition to colorimetric, fluorometric 0D chemical sensors are also highly sensitive.[56,92,105] The main employed
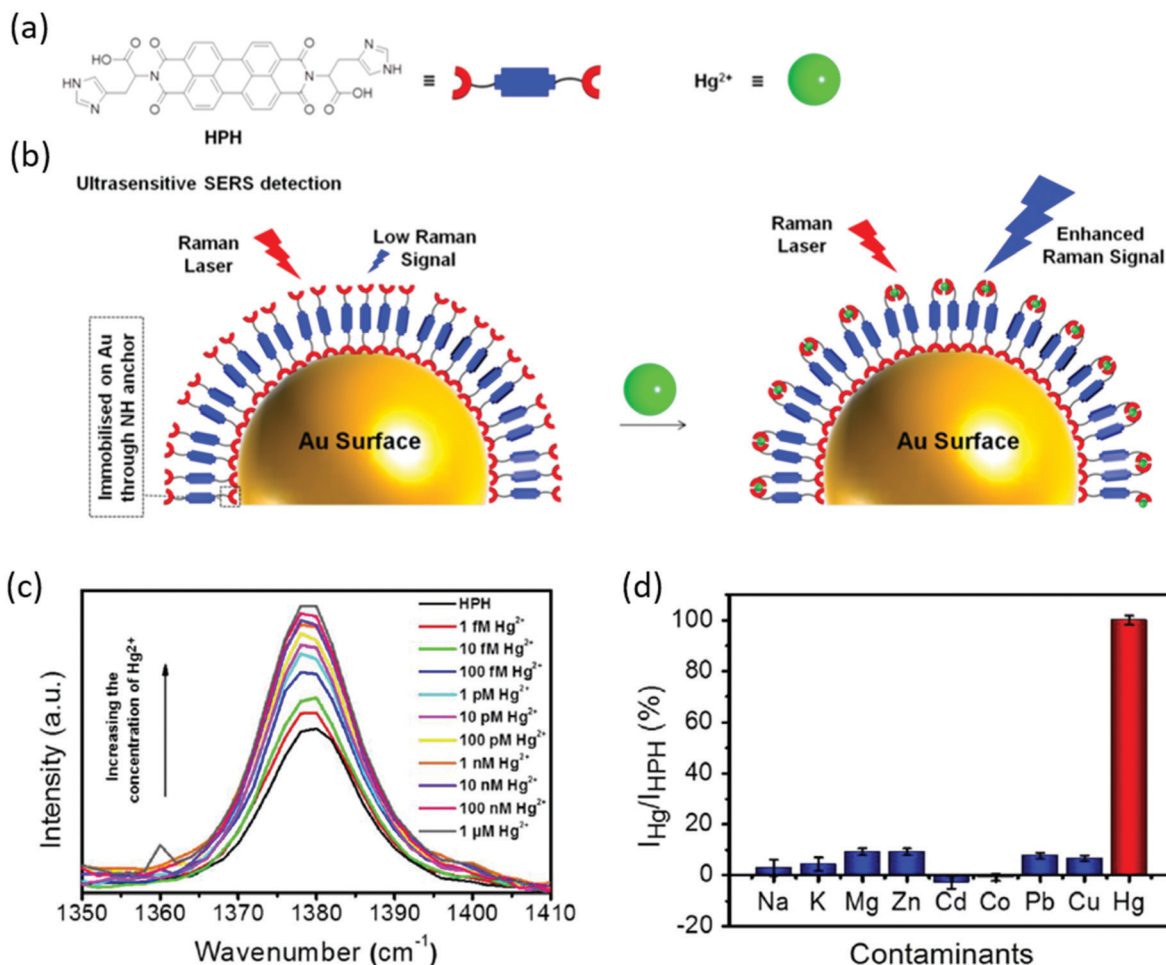
Fig. 5   0D Hg^{2+} SERS sensor in water based on HPH-functionalized Au NPs. (a) Chemical structures and corresponding schematic representations of HPH and Hg^{2+}. (b) Ultrasensitive SERS detection of Hg^{2+}; HPH anchors on Au−MNM *via* NH of imidazole from one of the histidine moieties that amplify the Raman signal of HPH upon complexation with Hg^{2+} and by the involvement of adjacent HPH molecules immobilized on the gold surface. (c) SERS peak at 1380 cm^{-1} of HPH marker upon addition of increasing concentrations of Hg^{2+}, (d) Selectivity of the Au−MNM−HPH toward Hg^{2+} (based on the characteristic Raman band at 1380 cm^{-1}) in the presence of other metal ion species in solutions containing 1 μM of each cation for an exposure period of 0.5 h. Adapted from ref. 96 with permission of Elsevier.

strategy relies on the complexation of the functionalized NPs with the target analyte, *e.g.*, ion or (bio)molecule, resulting in the quenching or restoration of the initial fluorescence of the system.[17] Sensors utilizing surface-enhanced Raman scattering (SERS) spectroscopy are equally powerful, allowing the ultra-sensitive detection of many species even at a single-molecule level.[115] When the analyte interacts with the specific receptor it modifies the Raman signals of the latter. SERS sensors combine appealing characteristics, such as "fingerprint" information, non-invasive and non-destructive identification, and compat-ibility with portable, on-the-spot qualitative sensing.[93,96,113] For example, Makam *et al.* reported a SERS sensor of Hg^{2+} in water by using Au NPs functionalized with histidine (H) conjugated perylene diimide (PDI) bolaamphiphile (HPH) (Fig. 5).[96] The SERS platform consisted of Au-deposited monodispersed nano-spheres monolayers (Au-MNM) of polystyrene fabricated by using e-beam evaporation. Since Hg^{2+} is divalent, it can chelate to neighbouring HPH molecules by forming HPH−Hg^{2+}

host–guest complex which triggers the enhancement of the Raman signal of the HPH ligands as a function of Hg^{2+} concentration (Fig. 5b). This simple and effective design prin-ciple of host–guest interactions driven SERS-based detection offers an unprecedented selectivity and the best reported LoD of 60 attomolar (aM, 0.01 parts-per-quadrillion (ppq) for Hg^{2+} in water (Fig. 5c and d).

0D materials are extensively used also in chemiresistors, where a NP network is integrated in between a pair of electro-des *via* controlled assembly mediated by molecular receptors. Molecule-NPs arrays comprise a class of chemiresistors known as MIMEs (metal–insulator–metal ensembles), where an insu-lating organic linker attached to the NP's surface provides stabilization of the whole structure, sites for the analyte adsorp-tion/binding, and sufficient electrical conductivity through the network. Chemical-to-electrical transduction occurs when the analyte enters the spaces between the NP cores, modulates the tunneling probability or the distance between them,
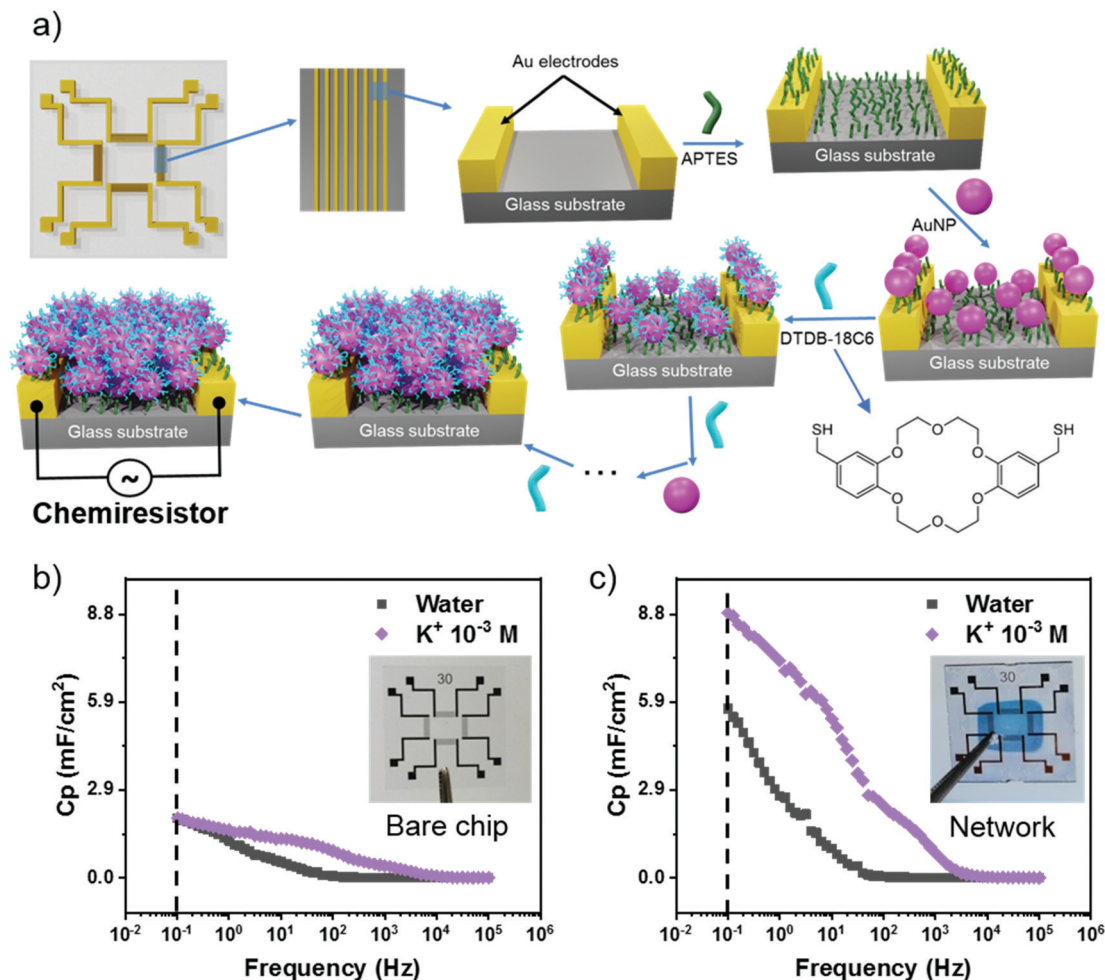
Fig. 6 0D electrical sensor-based of networks of Au NPs for K$^+$ sensing (a) Schematic layer-by-layer fabrication of CRs based on covalently assembled Au NPs-DTDB-18C6 networks, Capacitance response of (b) bare and (c) Au NPs-DTDB-18C6 network-coated IDEs in Milli Q water (black curves) and K$^+$ 10^{-3} M (violet curves). Inset: Respective pictures of the bare and network-coated glass chips. Adapted from ref. 98 with permission from Wiley-VHC.

thereby tuning the chemiresistor output current.[98,108] Despite the recent progress on chemiresistors with enhanced sensitivity, only a few sensors display high selectivity towards a specific analyte.[98] Recently, we have reported the fabrication of CRs based on 3D networks of Au NPs covalently bridged by *ad hoc* supramolecular receptors, namely dithiomethylene dibenzo-18-crown-6 ether (DTDB-18C6), for K$^+$ recognition *via* host–guest interactions. (Fig. 6a).[98] The sensor showed exceptional KPIs: (i) linear sensitivity in the 10^{-3} to 10^{-6} M concentration range; (ii) high selectivity to K$^+$ in presence of interfering cations (Na$^+$, Ca^{2+}, and Mg^{2+}); (iii) high shelf-life stability ($>$45 days); (iv) reversibility of K$^+$ binding and release; (v) successful device integration into microfluidic systems for real-time monitoring; (vi) fast response and recovery times ($<$18 s), and (v) K$^+$ detection in artificial saliva. From the capacitance (C_p)-frequency response of the network-coated interdigitated electrodes (IDEs), we observed that 0.1 Hz is the best frequency, where C_p increases by 443% in 10^{-3} M K$^+$, distinctively from C_p increase in water (283%) and the response of the bare chip (Fig. 6b and c).

Electrochemical sensors have been also developed by using 0D materials as active sensing materials. To illustrate that, we can refer to the work of Ran *et al.* who developed an electrochemical sensor for 2,4,6-trinitrotoluene (TNT) by depositing nitrogen-doped carbon quantum dots (N-CQDs) functionalized with pillar[6]arenes (WP6s) on a glass carbon electrode (GCE).[108] WP6s can effectively functionalize N-CQDs through π–π interactions and, due to the high (supra)molecular recognition capability of WP6 host towards TNT, can also enhance the electrochemical signal of the TNT reduction. A LoD of 0.95 nM and two linear ranges, 0.001–1.0 μM, and 1.0–20.0 μM, were achieved by using this simple electrochemical platform.

Sensors based on 1D LDMs

Typical transducing methods for 1D-based sensors include optical/photonic processes, mainly photoluminescence,[107,116–118] SPR,[119] and SERS,[9,62] and electrical/electrochemical operation (*viz.* chemiresistors, field-effect transistors (FETs), or modified electrodes). Optical (and photonic) properties and related signal transduction depend on diverse characteristics of 1D nanostructures. For example, single NWs can tightly confine
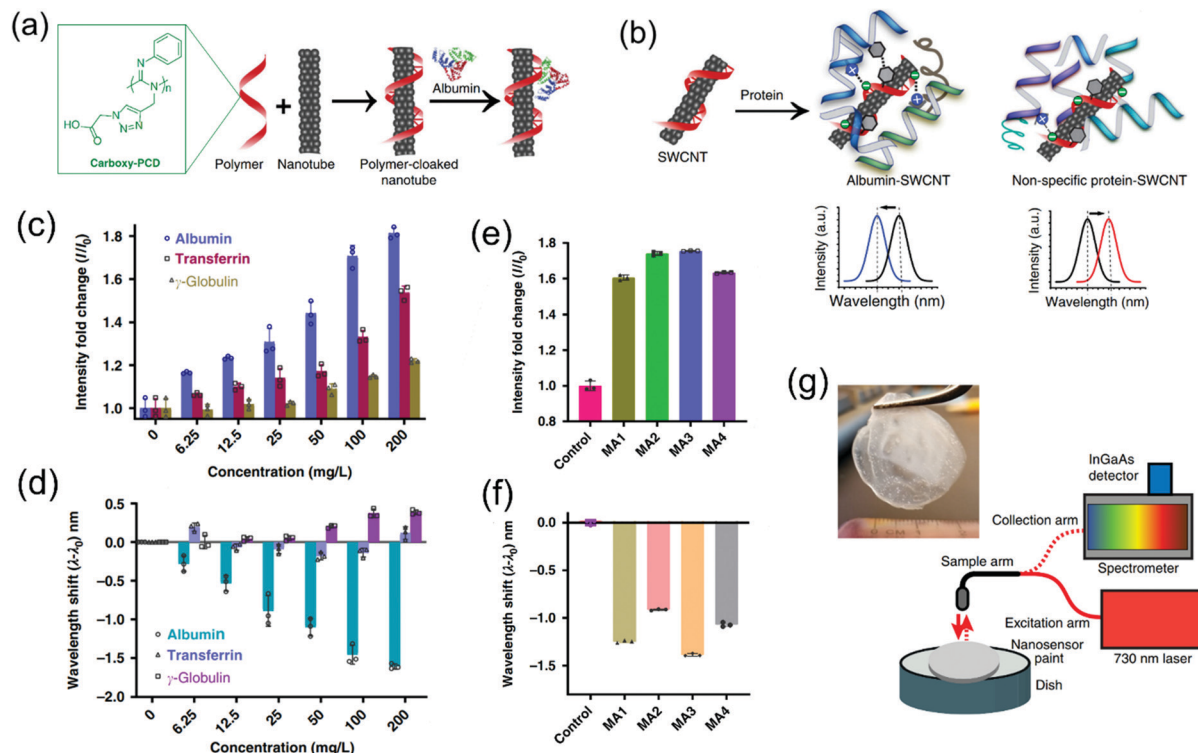
Fig. 7 Optical transduced 1D sensor based on polymer–functionalized SWCNTs for albumin detection. (a) Scheme of the SWCNT functionalization with a carbodiimide polymer. (b) Sensing mechanism and response for specific and non-specific protein interactions. (c and d) Sensor response (intensity change and wavelength shift, respectively) to albumin and interfering transferrin and γ-globulin proteins. (e and f). Sensor response to albumin in urine samples. (g) Free-standing nanosensor paint for PoC optical sensing. Adapted with permission from ref. 106 Copyright 2017 Nature Publishing Group.

light for enhanced light–matter interaction *via* evanescent fields at their surroundings, with properties dependent on the wavelength/NW diameter ratio and nature (*viz.* dielectric or metallic NWs). Individual NWs provide a small footprint and high spatial resolution, while aligned NW arrays can benefit from coupling and synergetic effects, exhibiting enhanced and also anisotropic optical properties.[120] Optical 1D chemical sensors based on CNTs rely mostly on the near-infrared photoluminescence of single-walled CNTs (SWCNTs), their distinctive Raman signals, and fluorescence quenching ability.[121,122] In general, interactions with the analyte that either changes the dielectric/chemical environment around NWs and NTs or cause charge transfer processes are the main mechanisms underpinning the operation of optical 1D sensors. One compelling example of optical transduction using 1D nanostructures is the nanosensor developed by Heller and co-workers to detect albumin in urine samples.[106] The sensor can detect albumin up to concentrations of 3 mg L^{-1}, which is compatible with standard immunoturbidimetric clinical assays (LoD of 1 mg L^{-1}). The strategy is based on the encapsulation of (9,4) chiral SWCNTs with a carboxylate-rich hydrophobic carbodiimide polymer (carboxy-PCD) synthesized to mimic fatty acid-binding to the albumin *via* hydrophobic and Coulomb interactions (Fig. 7a). Upon specific binding, a blue shift and strong intensity change in near-infrared photoluminescence are observed, while for non-specific protein interactions a redshift is produced (Fig. 7b). SWCNTs functionalized with amine-terminated or

polyethylene glycol–PCD showed no selectivity towards the analyte, highlighting the importance of the (supra)molecular interactions between the designed carboxy–PCD and albumin groups. The sensor selectivity is further demonstrated in the presence of potentially interfering proteins in urine, such as transferrin and γ-globulin, which produces an opposite wavelength shift and reduced intensity changes (Fig. 7c and d). The method can detect microalbuminuria – an important clinical marker of several diseases – in urine samples of patients (Fig. 7e and f). The polymer–SWCNT complex can also be incorporated into an acrylic material resulting in a free-standing paint for the development a PoC optical sensing technology.

For sensors having electrical readout, the interaction of NWs and NTs with analytes is accompanied by a modulation of their electrical properties, *e.g.*, *via* scattering electrons in metal NWs, by accepting/donating electrons in semiconducting nanostructures, by lowering interface barriers in devices, *etc.*[9] Electrical sensors employing individual 1D LDMs typically offer high sensitivity and fast responses upon interaction with a given analyte (including responsiveness to a single molecule).[123,124] However, they require complex and low-yield fabrication strategies when compared to networks, which are easier to be integrated into chips and display higher device-to-device reproducibility.[9,62] Aligned networks composed of 1D conducting LDMs will typically exhibit greater current densities when compared to randomly oriented networks due to longer
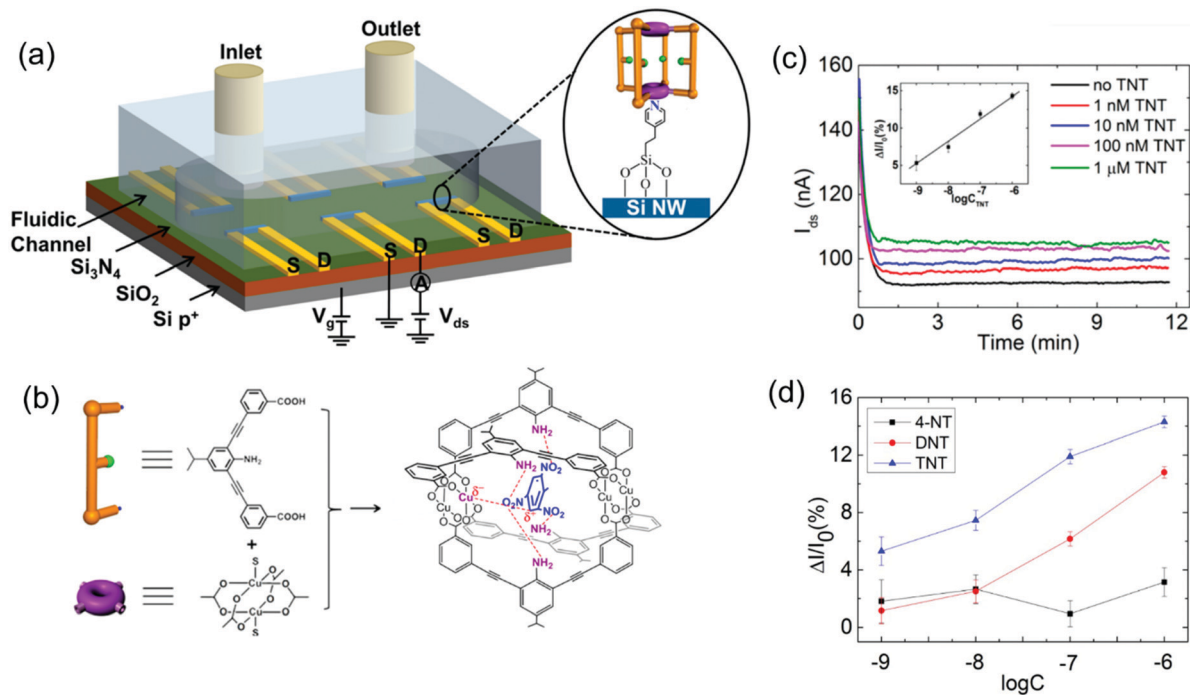
Fig. 8 Electrically transduced 1D-based sensor based on Si NW FETs functionalized with pyridyl–silane linker and a metal–organic polyhedral (MOP) receptor for the detection of 2,4,6-trinitrotoluene (TNT) explosive. (a) Chip schematics having electrical connections and a microfluidic channel. (b) Chemical composition of the MOP constituents and the modeling of TNT molecule trapping into the MOP cage. (c) Time-dependent source–drain current characteristics for the MOP–Si NW FET at different concentrations of TNT ethanolic solutions. Inset: Respective calibration curve. (d) Relative current change *versus* the explosive concentrations (*viz.* TNT, DNT, and 4-NT). Adapted with permission from ref. 109 Copyright 2017 American Chemical Society.

mean-free path for electron conduction. However, randomly oriented networks possess the advantage of porosity with higher surface area for greater interaction with analyte species. To illustrate the development of electrical sensors based on 1D nanostructures, let us consider the work of Cao *et al.* for the detection of trace explosives.[109] FETs made of individual p-type Si NWs were functionalized with a 2-(4-pyridylethyl)-triethoxysilane monolayer and Cu-based metal−organic poly-hedral (MOP) cages (Fig. 8a and b). The devices are embedded into a microfluidic chip used to deliver explosive-containing solutions by varying concentrations (from 1 nM to 1 μM) to the sensor's surface. The FET source–drain current (I_{DS}) was recorded over time at a fixed gate and drain bias. The device's relative steady-state current ($\Delta I/I_0$) shows a linear relationship with the logarithmic analyte (2,4,6-trinitrotoluene, TNT) concentration, reaching a LoD of 100 pM (Fig. 8c). The sensor is selective to TNT, exhibiting weaker or null responses to structurally similar molecules, such as 2,4-dinitrotoluene (2,4-DNT) and 4-nitrotoluene (4-NT) as depicted in Fig. 8d. In the absence of the Cu–MOP cage, the device responds to TNT with sensitivity 3 orders of magnitude lower, highlighting the impor-tance of the receptor on the (supra)molecular recognition. DFT computational studies revealed that one MOP cage can accom-modate only one TNT molecule due to size fit. Additionally, two NO_2 groups of the TNT molecule interact (*via* hydrogen bond-ing) with the available two NH_2 groups of the Cu–MOP, while the third nitro group points to two NH_2 groups with the line

formed by the four Cu^{2+} ions of the Cu–MOP penetrating the aromatic ring of the TNT molecule (Fig. 8b). The observed current increase in the FETs results from an increased negative electrical potential at the surface of the p-doped SiNWs due to the interaction between the trapped TNT molecule and the adjacent copper ion in the receptor. This leads to the formation of a net dipole moment of the TNT-receptor complex pointing towards the surface that modifies the device band bending, ultimately leading to higher channel currents/conductance.[109]

Electrochemical sensors also take great advantage of the remarkable electrical properties of some 1D nanostructures, such as CNTs. Alam *et al.*, for example, developed a simple, and low-cost electrochemical sensor based on multi-walled CNTs (MWCNTs) functionalized with β-cyclodextrin (β-CD) to detect lead (Pb^{2+}) in drinkable water.[97] β-CD was employed to both improve the dispersion of the CNTs and to serve as a receptor for the target analyte. Two functionalization strategies have been tested, one relying on the physisorption (Phys) of β-CDs onto the MWCNTs and another based on the covalent attach-ment of β-CDs *via* the Steglich esterification (SE) of COOH-terminated MWCNTs (Fig. 9a). After functionalization, both MWCNT-βCD(Phys) and MWCNT-βCD(SE) were drop-casted onto screen-printed electrodes (SPEs) and the sensing experi-ments were performed using differential pulse anodic stripping voltammetry (DPASV). Fig. 9b shows the voltammogram and its respective linear calibration curve for the MWCNT-βCD(Phys)/SPE sensor in the presence of 0.025–20 μM (3.1–103.3 ppb)
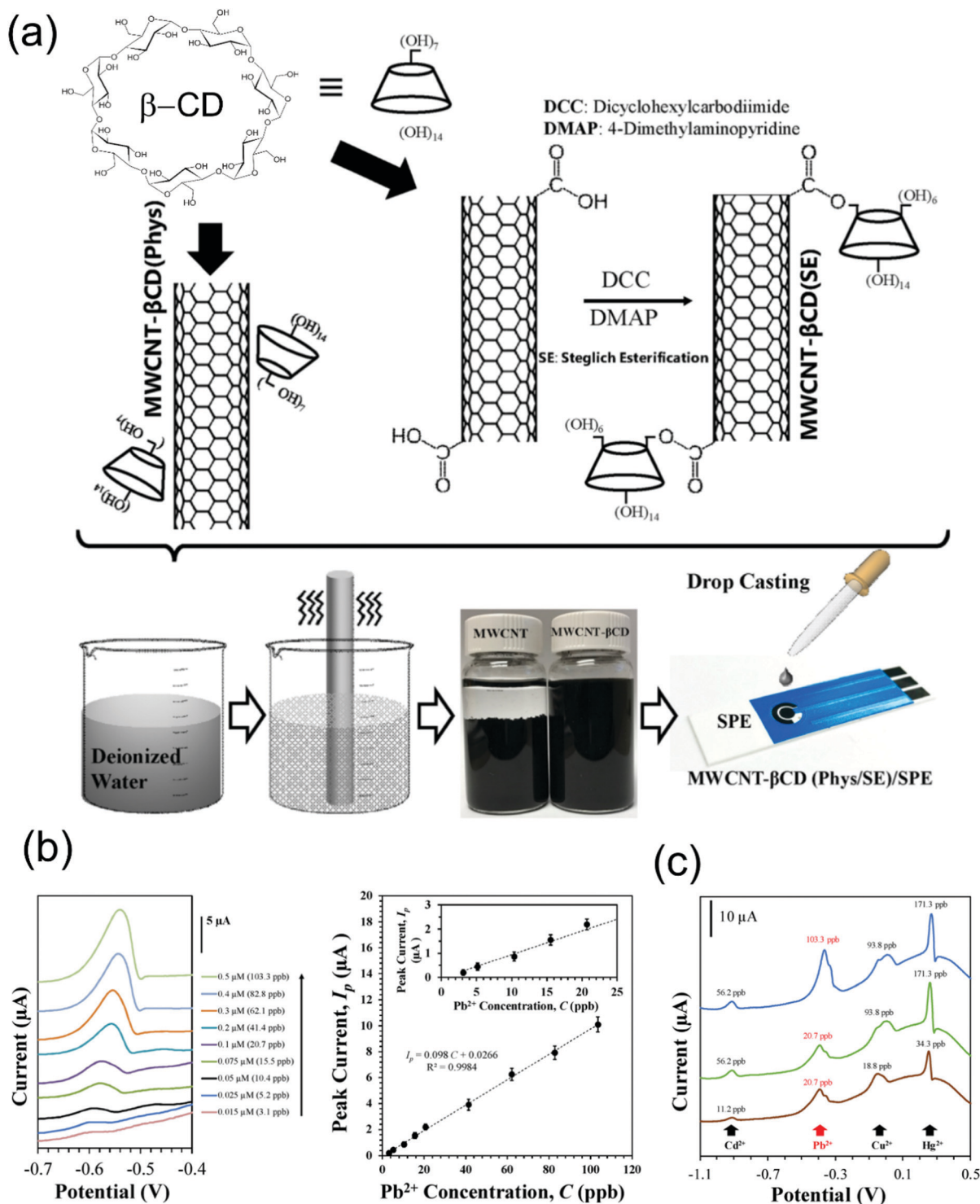
Fig. 9 1D electrochemical sensor based on MWCNTs functionalized with β-cyclodextrin (β-CD) receptors. (a) Schematics of the MWCNTs functionalization with β-CD *via* two routes, *viz.* physisorption and covalent bonding. (b) Sensor stripping voltammogram and respective calibration curve at varied Pb²⁺ concentrations. (c) Sensor selective response to Pb²⁺ in the presence of interfering cations. Adapted from ref. 97 with permission of Elsevier.

Pb^{2+}, after the Pb^{2+} preconcentration at a deposition potential of -0.8 V for 600 s to form Pb^0. The MWCNT-βCD(Phys)/SPE sensor can detect Pb^{2+} with a LoD of 0.9 ppb with a sensitivity of 98 nA ppb^{-1}. The sensor based on the covalent functionalization strategy, *i.e.* MWCNT-βCD(SE), is 2.5 times less sensitive

and exhibited a LoD of 2.3 ppb, probably due to the fewer unit of grafted β-CD limiting the number of available COOH sites for the functionalization. However, this strategy has shown to be more robust and allows sensor reuse. The reported sensor can also detect Pb^{2+} in the presence of interfering cations as

illustrated in Fig. 9c. The device can detect 0.1 μM of Pb^{2+} in spiked drinkable water with >90% overall recovery.[97]

Sensors based on 2D LDMs

Like their 0D and 1D counterparts, sensors employing functionalized 2D materials rely mostly on optical, electrical, and electrochemical transduction. While GO and rGO functionalized with macrocyclic receptors can enable or enhance electron transfer processes between the recognized guest analyte and an electrode in electrochemical sensors,[125,126] they can also act as a donor or acceptor in fluorescence resonance energy transfer (FRET)-based optical sensors.[17] To illustrate the functionalization of rGO for optical sensing we can consider the work of Zhao et al.[112] on the competitive fluorescence detection of acetaminophen (AP) or paracetamol, one of the most common medicine for treating pain and fever (Fig. 10). Amphiphilic pillar[5]arene (amPA5) functionalized rGO can quench the fluorescence of a signal probe (acridine orange, AO) thanks to the AO accommodation into the amPA5 cavity and the strong quenching ability of rGO (Fig. 10a and b). Upon titration of the target molecule (AP), the fluorescence is recovered (switch on)

by the displacement of the AO indicator from the amPA5 host (Fig. 10c). The fluorescence response is proportional to the AP concentration, exhibiting two linear regimes ranging from 0.1–4.0 and 4.0–32.0 μM, with a LoD of 0.05 μM (Fig. 10d). The method has shown to be highly specific to the AP molecule in respect to common interfering molecules (Fig. 10e). Molecular docking studies (Fig. 10b) revealed that hydrogen bonding between the O13 atom of amPA5 and the N atom of AP, electrostatic interactions between the negatively charged acetyl O atom and the NH_3^+ of AP, and π–π interactions between their benzene rings are the main interactions governing the (supra)molecular recognition of the analyte (Fig. 10b). Finally, AP was also detected in human serum samples.

Sensing with graphene is commonly achieved by electronic transducers, e.g. chemiresistors, solid-state FETs, and liquid-gated transistors (LGTs), where the receptor-analyte interaction occurring on the graphene surface is converted into changes on the device's electrical characteristics (e.g. channel conductivity, charge carrier mobility, Dirac point voltage, etc.).[10,127,128] Graphene LGTs were recently employed to develop one of the first biosensors for the detection of SARS-CoV-2 virus responsible for the COVID-19 global pandemic.[129,130] To illustrate the use of graphene transistors sensors employing (supra)molecular
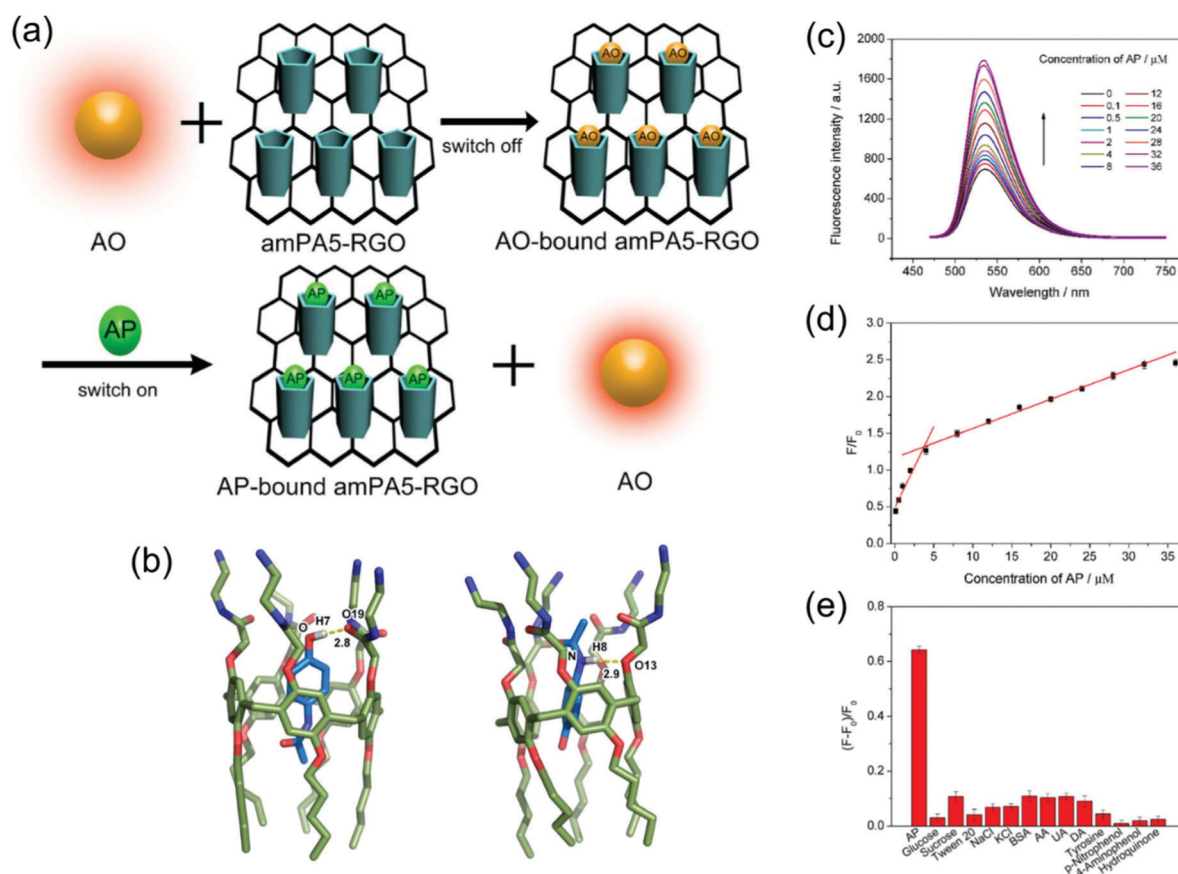
Fig. 10 2D optical sensor for the detection of acetaminophen (AP) – paracetamol – using rGO functionalized with amphiphilic pillar[5]arene (amPA5) receptors. (a) Schematics of the competitive fluorescent approach using an acridine orange (AO) indicator. (b) AP/amPA5 complex by molecular docking. (c) Fluorescence spectra of the AO·amPA5-RGO complex upon increasing concentrations of AP (0–36 μM), and (d) its respective calibration curve. (e) Relative fluorescence intensity for AP and common interfering molecules. Adapted from ref. 112 with permission of Elsevier.
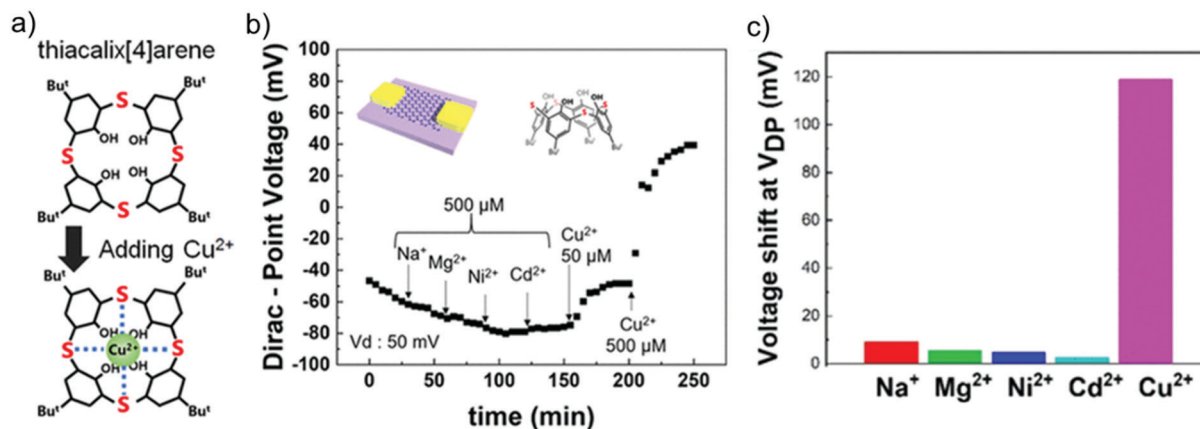
Fig. 11 2D electrical sensor based on graphene for the detection of Cu^{2+}. (a) Chemical structure of thiacalix[4]arene receptors for the recognition of Cu^{2+} ions. (b) Real-time detection of Cu^{2+} via monitoring of the Dirac Point voltage of functionalized graphene TFTs (inset: device sketch). (c) Selective Cu^{2+} sensing and device response in the presence of interfering cations. Adapted with permission from ref. 74 Copyright 2020 American Chemical Society.

receptors we can refer to the work of Takagiri *et al.* for the selective detection of Cu^{2+}.[74] Thiacalix[4]arene (TCA) receptors were immobilized on the graphene surface *via* π–π stacking (Fig. 11a). Upon exposure to different Cu^{2+} concentrations (1, 10, 30,100, and 300 μM) the functionalized graphene transistors respond with systematic shifts of the Dirac-point voltage towards more positive potentials,[74] which can also be monitored in real-time (Fig. 11b). This results from the selective Cu^{2+} hosting by the TCA receptors that induces the accumulation of electrons on the graphene surface, which does not occur for other cationic species such as K^+, Mg^{2+}, Ni^{2+}, and Cd^{2+} even at higher concentrations (Fig. 11c). According to the authors, the recognition of Cu^{2+} employing TCA immobilized on graphene can be explained using the hard and soft acids and bases (HSAB) theory and the ligand field theory, where soft metal ions (Cu^{2+}, Ni^{2+}, and Cd^{2+}) tend to easily coordinate with sulphur atoms. In this work, however, the device responds only to Cu^{2+} and not to Ni^{2+} and Cd^{2+}, which can be due to the TCA planar configuration on the graphene surface. For free TCA receptors in solution, they coordinate with other metal cations, loosing the particular Cu^{2+} selectivity.[74]

Regarding non-graphene 2DMs, one interesting example is the BP electrochemical sensor recently reported by Zou and You for the chiral discrimination of tryptophan (Trp) enantiomers.[88] Exfoliated BP nanosheets (BPNSs) functionalized with 6-O-α-maltosyl-β-cyclodextrin (G2-β-CD) in solution were drop-casted on a glassy carbon electrode (GCE) and stabilized with Nafion (NF), as shown in Fig. 12a. The electrochemical chiral recognition of Trp enantiomers was performed using the NF/BPNSs-G2-β-CD/GCE modified electrode utilising square wave voltammetry (SWV). The authors verified that the SWV peak potential (Ep) and peak current response (I) of L-Trp and D-Trp were different, allowing their successful discrimination (Fig. 12b). They found signal ratios of $I_L/I_P = 1.49$ and $\Delta E_p = 20$ mV, at fixed Trp concentration (1 mM) that characterize the sensor stereospecificity to the target Trp enantiomers, as shown in Fig. 12c. Other amino acids, such as tyrosine (Tyr), histidine (His) and phenylalanine (Phe) do not produce the same signal

response (Fig. 12c). Regarding the variation of the L- and D-Trp concentration (0.01–1 mM), the sensor KPIs include sensitivity and LoD, respectively, of 21.09 μA mM^{-1} and 1.07 μM (L-Trp) and 13.25 μA mM^{-1} and 1.71 μM (D-Trp). Discrimination of Trp enantiomers is claimed to be due to the specific host-size matching between the G2-β-CD receptor and each Trp isomer and the hydrogen-bonding interactions formed between them (given the suitable intermolecular distances) in each case (Fig. 12d).

Likewise graphene, most applications based on TMDs, BP, and MXenes for sensing where the recognition of analytes is achieved by (supra)molecular interactions refer to biosensors.[65,131] Noteworthy examples include TMD transistors,[132,133] electrochemical and optoelectronic devices,[134,135] and fluorescence/colorimetric indicators, BP transistors,[136,137] MXene-modified electrodes[138,139] and SPR chips[139] decorated with bioreceptors (*e.g.* antibodies, aptamers, *etc.*) for the detection of disease biomarkers. While biosensors inherently possess elevated selectivity, synthetic recognition elements generally hold improved stability, reduced costs, and chemical flexibility to be modified according to desired LDM, device surface type, the solvent employed, *etc.* The biggest challenge of (supra)molecular chemistry applied for sensing is to create synthetic recognition elements that can mimic the natural analyte-receptor interaction with high affinity especially in harsh conditions, such as in a physiological environment. In this matter, the literature reveals that 2DM-based sensors employing selective chemical receptors still have a long way ahead in comparison to their 0D and 1D counterparts. General drawbacks that hinder more practical sensing applications comprising 2DMs are the absence of established protocols for the mass production of high-quality and wafer-scale materials, the lack of facile and effective strategies for their integration into devices, and the limited environmental stability for some 2DMs (*e.g.* BP).[140] The impact of chemical functionalization on the material's properties and the role of structural defects on the sensing performance are some of the hurdles and major challenges to be addressed using such 2DMs. The field of
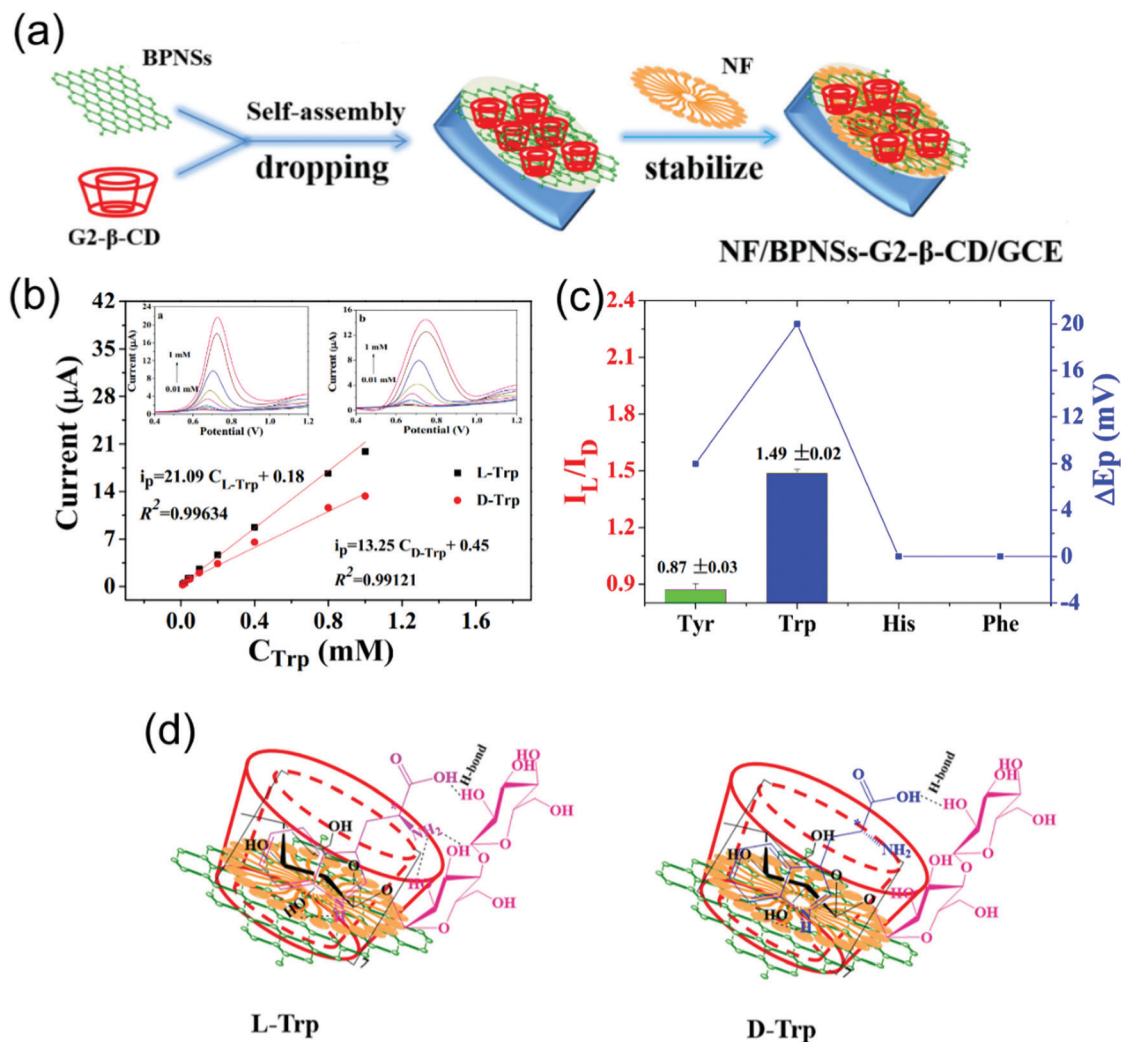
Fig. 12 2D BP-based electrochemical sensing for enantiomeric discrimination. (a) Fabrication of the modified glassy carbon electrodes (GCE) with BP nanosheets functionalized with G2-β-CD and stabilized with Nafion (NF). (b) Sensor electrochemical response to D- and L-tryptophan (Trp). (c) Sensor current and potential ratio for the enantiomeric discrimination of Trp and other amino acids. (d) Illustration of the L-Trp L-Trp and D-Trp accommodation into the chiral selective cavity of the employed G2-β-CD receptor. Adapted from ref. 88 with permission of Elsevier.

chemical sensing with 2DMs is still in its infancy and the exploitation of the broad chemical and structural diversity of the whole plethora of 2DMs is fundamental to further expand possibilities in this field. In this regard, the emerging class of 2D metal–organic[141] and covalent organic frameworks[142] (MOFs and COFs, respectively)[143] holds great promises to out-perform naturally occurring 2DMs. Their composition, struc-ture, physical and chemical properties as well as functionalities can be chemically engineered during synthesis and/or assembly and translated into the device operation.

Selective analyte recognition: from laboratory to real applications

Despite the tremendous effort made by the scientific commu-nity to develop highly selective chemical sensors, there is no universal list where one can find the best receptor for a given analyte. As shown in Table 1, for some analytes (*e.g.* Cu^{2+} or TNT) different receptors have been reported selective in the presence of interfering compounds. In some cases, these receptors have similar chemical structures, hence interacting with an analyte similarly. However, in other cases, the struc-tures of the receptors are completely different, for example, the use of *p*-aminobenzenethiol and water-soluble pillar[6]arene for TNT sensing. Likewise, the very same receptor has been used to selectively detect completely different analyte species. For example, β-cyclodextrin has been used for the detection of Pb^{2+}, dopamine, acetaminophen, 17β-estradiol, and the enan-tiomeric discrimination of tryptophan and other 19 amino acids. This is not impeditive for practical applications, as long as selectivity is demonstrated upon the appropriate choice of interfering compounds. Not only analytes with similar chemical structures to the analyte of interest should be evaluated but also interfering species found in real matrices. Alongside, different environmental conditions (*e.g.*, pH,

humidity, temperature, physiological conditions, *etc.*) can influence the analyte-receptor interaction and hence chemical sensors should be assessed in analogous environments to that of the real applications.

Summary and outlook

We presented the key concepts and greatest challenges for harnessing the selectivity of sensing technologies by using LDM functionalization and analyte (supra)molecular recognition. By taking full advantage of the synergetic combination of LDMs with *ad hoc* receptors, one can design and produce the next generation of sensory materials and technologies exhibiting designed analyte selectivity along with unprecedented KPIs, such as LoDs down to sub-ppb level, and fast, accurate, and reversible responses. As diverse signal transducers are available (optical, electrical, and electrochemical devices), with a multitude of operating modes and signal readout. The choice for the optimal sensing technology relies on the specific dynamic physical property of the chosen nanostructure, which is utilized to transduce the analyte-receptor interaction. Analyte recognition is achieved *via* one or more non-covalent interactions (*e.g.*, hydrogen-bonding, metal–ligand bonding, van der Waals and electrostatic interactions, or hydrophobic forces) endowed by a great variety of natural or synthetic receptors attached directly on the LDM surface. Alternative approaches to attain selectivity *via* (supra)molecular recognition include more complex receptor formulations, such as ion-selective membranes (ISMs)[144–146] and molecular imprinted polymers (MIPs).[147–150] However, these may suffer from adventitious interference of molecules structurally similar to the target analyte.[150] In the future, the use of machine learning approaches to enable rational design and high-throughput screening of large libraries of molecules as potential receptors for the analyte of choice holds a huge potential to boost selectivity. Comparative studies employing the very same receptor but different LDM and/or transducing devices would help one to understand the potential and limits of each sensing technology, aiming their optimization.

Despite the major progress on the LDMs production, control of properties, and sensor proof-of-concept demonstrations, there are still some issues that must be addressed urgently to exploit their potential in everyday applications. From a technological perspective, important challenges refer to the establishment of industrial-scalable and affordable manufacturing methods to either produce novel sensors able to meet the high standards required for commercialization or to integrate LDMs into existing mature technologies. This involves the production of sensors that are ultimately robust, affordable, lightweight, small, stable, user-friendly, and exhibit low power consumption. Additional challenges to upgrade LDMs from prototype to commercial sensing technologies include the production of high-quality materials at accessible prices, robust functionalization methods compatible with industrial practices, and long-term sensor reliability operating in real and harsh environments (*e.g.*, high/low humidity or temperature, or in physiological conditions).

The lack of facile and efficient protocols to incorporate functionalized LDMs into transducing platforms represents another important hurdle. Lab batch reactions are straightforward and reliable, but frequently LDM transfer to real device platforms is seldom achieved. Issues regarding the sensor operation which are important to be addressed are related to signal drift or fluctuation, persistent accuracy, simple calibration methods, long-term stability, and shelf-lifetime. Significantly, challenges and aspects of technological order targeted for the development and optimization of chemical sensors can also be extended to other types of sensors, such as humidity, strain, and pressure sensors, for instance.

Like a sommelier in a blind wine tasting, the biggest challenge in chemical sensing – even for present commercial devices – refers to the unguided detection, where the identification and/or quantification of a given compound in a complex real sample is performed without previous information about its composition. Another major task in chemical sensing consists in the simultaneous determination of multiple analytes in complex media (*e.g.*, chemical or biological markers in blood, urine, serum, *etc.*). For this purpose, a possible strategy envisions the use of sensor arrays for multiplex sensing, each of them bearing a different functionalized LDM, able to acquire multivariate data (*i.e.*, more than one output signal or sensor parameter). Computerized statistical treatment and artificial intelligence resources (*e.g.*, machine learning) could be used to process a large amount of data into interpretable information (Big Data Analytics).

The deployment of industrial-compatible manufacturing of high-quality materials (*e.g.* wafer-scale LDMs) and devices (*e.g.* roll-to-roll printing), the use of microfluidic systems to handle small amounts of multiple analytes, and the fabrication of wearable (*e.g.* bands or plasters), disposable platforms (*e.g.* test strips), or substrates engineered to present strong optoelectronic coupling,[151,152] are some of the routes to proceed towards affordable and/or novel sensing technologies. We hope that all discussed strategies on how to harness the performance of chemical sensors based on LDMs and their current challenges can encourage researchers in the field to pursue novel and improved technological applications. We strongly believe that chemical sensing can aid several sectors of our society, offering solutions to issues in (bio)chemical defense, environmental and food surveillance, industrial safety, and medical (early) diagnostics, ultimately improving the quality of our lives on this planet.

Conflicts of interest

The authors declare no conflict of interest.

Acknowledgements

References

1 W. J. Peveler, M. Yazdani and V. M. Rotello, *ACS Sens.*, 2016, **1**, 1282–1285.

2 J. Mosquera, Y. Zhao, H. J. Jang, N. L. Xie, C. L. Xu, N. A. Kotov and L. M. Liz-Marzán, *Adv. Funct. Mater.*, 2020, **30**, 1902082.

3 E. Singh, M. Meyyappan and H. S. Nalwa, *ACS Appl. Mater. Interfaces*, 2017, **9**, 34544–34586.

4 V. Montes-García, M. A. Squillaci, M. Diez-Castellnou, Q. K. Ong, F. Stellacci and P. Samorì, *Chem. Soc. Rev.*, 2021, **50**, 1269–1304.

5 G. Maduraiveeran, M. Sasidharan and V. Ganesan, *Biosens. Bioelectron.*, 2018, **103**, 113–129.

6 R. Das, C. D. Vecitis, A. Schulze, B. Cao, A. F. Ismail, X. Lu, J. Chen and S. Ramakrishna, *Chem. Soc. Rev.*, 2017, **46**, 6946–7020.

7 Z. Li, H. Li, Z. Wu, M. Wang, J. Luo, H. Torun, P. Hu, C. Yang, M. Grundmann, X. Liu and Y. Fu, *Mater. Horiz.*, 2019, **6**, 470–506.

8 N. Rohaizad, C. C. Mayorga-Martinez, M. Fojtů, N. M. Latiff and M. Pumera, *Chem. Soc. Rev.*, 2021, **50**, 619–657.

9 V. Schroeder, S. Savagatrup, M. He, S. B. Ling and T. M. Swager, *Chem. Rev.*, 2019, **119**, 599–663.

10 Z. Meng, R. M. Stolz, L. Mendecki and K. A. Mirica, *Chem. Rev.*, 2019, **119**, 478–598.

11 C. Anichini, W. Czepa, D. Pakulski, A. Aliprandi, A. Ciesielski and P. Samorì, *Chem. Soc. Rev.*, 2018, **47**, 4860–4908.

12 X. Sun and Y. Lei, *Trends Anal. Chem.*, 2017, **89**, 163–180.

13 R. Ahmad, T. Mahmoudi, M.-S. Ahn and Y.-B. Hahn, *Biosens. Bioelectron.*, 2018, **100**, 312–325.

14 V. Cooper, C. Lam, Y. Wang and B. Sumpter, in *Non-Covalent Interactions in Quantum Chemistry and Physics: Theory and Applications*, ed. G. A. DiLabio and A. O. de la Roza, Elsevier, 2017, pp. 417–451.

15 G. Presnova, D. Presnov, V. Krupenin, V. Grigorenko, A. Trifonov, I. Andreeva, O. Ignatenko, A. Egorov and M. Rubtsova, *Biosens. Bioelectron.*, 2017, **88**, 283–289.

16 C. Dincer, R. Bruch, E. Costa-Rama, M. T. Fernández-Abedul, A. Merkoçi, A. Manz, G. A. Urban and F. Güder, *Adv. Mater.*, 2019, **31**, 1806739.

17 T. L. Mako, J. M. Racicot and M. Levine, *Chem. Rev.*, 2019, **119**, 322–477.

18 W. Gao, S. Emaminejad, H. Y. Y. Nyein, S. Challa, K. Chen, A. Peck, H. M. Fahad, H. Ota, H. Shiraki, D. Kiriya, D.-H. Lien, G. A. Brooks, R. W. Davis and A. Javey, *Nature*, 2016, **529**, 509–514.

19 E. S. Cho, J. Kim, B. Tejerina, T. M. Hermans, H. Jiang, H. Nakanishi, M. Yu, A. Z. Patashinski, S. C. Glotzer, F. Stellacci and B. A. Grzybowski, *Nat. Mater.*, 2012, **11**, 978–985.

20 V. M. Mirsky and A. K. Yatsimirsky, *Artificial Receptors for Chemical Sensors*, Wiley, 2010.

21 T. Schrader and A. D. Hamilton, *Functional Synthetic Receptors*, Wiley, 2005.

22 E. Er, H.-L. Hou, A. Criado, J. Langer, M. Möller, N. Erk, L. M. Liz-Marzán and M. Prato, *Chem. Mater.*, 2019, **31**, 5725–5734.

23 G. L. Long and J. D. Winefordner, *Anal. Chem.*, 1983, **55**, 712A–724A.

24 J. L. A. Jonathan and W. Steed, 2009.

25 D. E. O. T. E. P. A. O. T. C. O. D. O. T. Q. O. W. I. F. H. Consumption, *Off. J. Eur. Communities: Legis.*, 2020, **435**, 1–62.

26 L. Cui, Y. Wang, L. Gao, L. Hu, L. Yan, Q. Wei and B. Du, *Chem. Eng. J.*, 2015, **281**, 1–10.

27 M. A. Deshmukh, R. Celiesiute, A. Ramanaviciene, M. D. Shirsat and A. Ramanavicius, *Electrochim. Acta*, 2018, **259**, 930–938.

28 S. J. S. Flora and V. Pachauri, *Int. J. Environ. Res. Public Health*, 2010, **7**, 2745–2788.

29 A. Malek, K. Bera, S. Biswas, G. Perumal, A. K. Das, M. Doble, T. Thomas and E. Prasad, *Anal. Chem.*, 2019, **91**, 3533–3538.

30 R. D. Hancock and A. E. Martell, *Chem. Rev.*, 1989, **89**, 1875–1914.

31 N. J. Williams, N. E. Dean, D. G. VanDerveer, R. C. Luckay and R. D. Hancock, *Inorg. Chem.*, 2009, **48**, 7853–7863.

32 L. E. Tucker, G. C. Littman, S. Uritis, J. W. Nugent, R. P. Thummel, J. H. Reibenspies, S. B. Jones, H.-S. Lee and R. D. Hancock, *Inorg. Chem.*, 2020, **59**, 13117–13127.

33 G. M. Cockrell, G. Zhang, D. G. VanDerveer, R. P. Thummel and R. D. Hancock, *J. Am. Chem. Soc.*, 2008, **130**, 1420–1430.

34 R. D. Hancock, *Chem. Soc. Rev.*, 2013, **42**, 1500–1524.

35 A. Rakshit, K. Khatua, V. Shanbhag, P. Comba and A. Datta, *Chem. Sci.*, 2018, **9**, 7916–7930.

36 E. Kawabata, K. Kikuchi, Y. Urano, H. Kojima, A. Odani and T. Nagano, *J. Am. Chem. Soc.*, 2005, **127**, 818–819.

37 H. Najarzadekan and H. Sereshti, *J. Mater. Sci.*, 2016, **51**, 8645–8654.

38 D. Tsoutsi, L. Guerrini, J. M. Hermida-Ramon, V. Giannini, L. M. Liz-Marzán, A. Wei and R. A. Alvarez-Puebla, *Nanoscale*, 2013, **5**, 5841–5846.

39 I. Bhowmick, D. J. Boston, R. F. Higgins, C. M. Klug, M. P. Shores and T. Gupta, *Sens. Actuators, B*, 2016, **235**, 325–329.

40 P. D. Beer and J. Cadman, *Coord. Chem. Rev.*, 2000, **205**, 131–155.

41 L. Ward, A. Agrawal, A. Choudhary and C. Wolverton, *Npj Comput. Mater.*, 2016, **2**, 16028.

42 W. A. Christinelli, F. M. Shimizu, M. H. M. Facure, R. Cerri, O. N. Oliveira Jr., D. S. Correa and L. H. C. Mattoso, *Sens. Actuators, B*, 2021, **336**, 129696.

43 K. Shiba, R. Tamura, T. Sugiyama, Y. Kameyama, K. Koda, E. Sakon, K. Minami, H. T. Ngo, G. Imamura, K. Tsuda and G. Yoshikawa, *ACS Sens.*, 2018, **3**, 1592–1600.

44 S. Chaube, S. Goverapet Srinivasan and B. Rai, *Sci. Rep.*, 2020, **10**, 14322.

45 G. R. Schleder, A. C. M. Padilha, C. M. Acosta, M. Costa and A. Fazzio, *J. Phys. Mater.*, 2019, **2**, 032001.

46 R. Ouyang, E. Ahmetcik, C. Carbogno, M. Scheffler and L. M. Ghiringhelli, *J. Phys. Mater.*, 2019, **2**, 024002.

47 M. Teresa Albelda, J. C. Frías, E. García-España and H.-J. Schneider, *Chem. Soc. Rev.*, 2012, **41**, 3859–3877.

48 N. Busschaert, C. Caltagirone, W. Van Rossom and P. A. Gale, *Chem. Rev.*, 2015, **115**, 8038–8155.

49 E. J. Dale, N. A. Vermeulen, M. Juríček, J. C. Barnes, R. M. Young, M. R. Wasielewski and J. F. Stoddart, *Acc. Chem. Res.*, 2016, **49**, 262–273.

50 M. A. Zwijnenburg, E. Berardo, W. J. Peveler and K. E. Jelfs, *J. Phys. Chem. B*, 2016, **120**, 5063–5072.

51 M. Levine, *Front. Chem.*, 2021, **9**, DOI: 10.3389/fchem.2021.616815.

52 R. Wang, K.-Q. Lu, Z.-R. Tang and Y.-J. Xu, *J. Mater. Chem. A*, 2017, **5**, 3717–3734.

53 M. Azharuddin, G. H. Zhu, D. Das, E. Ozgur, L. Uzun, A. P. F. Turner and H. K. Patra, *Chem. Commun.*, 2019, **55**, 6964–6996.

54 C. D. De Souza, B. R. Nogueira and M. E. C. M. Rostelato, *J. Alloys Compd.*, 2019, **798**, 714–740.

55 A. S. Karakoti, R. Shukla, R. Shanker and S. Singh, *Adv. Colloid Interface Sci.*, 2015, **215**, 28–45.

56 R. Rani, Mayank, P. Thangarasu and N. Singh, *ACS Appl. Nano Mater.*, 2019, **2**, 1–5.

57 T. Han, Y. Yuan, X. Liang, Y. Zhang, C. Xiong and L. Dong, *J. Mater. Chem. C*, 2017, **5**, 4629–4635.

58 C. Cao, Y. Zhang, C. Jiang, M. Qi and G. Liu, *ACS Appl. Mater. Interfaces*, 2017, **9**, 5031–5049.

59 J. Oliver-Meseguer, M. Boronat, A. Vidal-Moya, P. Concepción, M. Á. Rivero-Crespo, A. Leyva-Pérez and A. Corma, *J. Am. Chem. Soc.*, 2018, **140**, 3215–3218.

60 J. Oliver-Meseguer, A. Doménech-Carbó, M. Boronat, A. Leyva-Pérez and A. Corma, *Angew. Chem., Int. Ed.*, 2017, **56**, 6435–6439.

61 K. Varga, S. Tannir, B. E. Haynie, B. M. Leonard, S. V. Dzyuba, J. Kubelka and M. Balaz, *ACS Nano*, 2017, **11**, 9846–9853.

62 J. F. Fennell, S. F. Liu, J. M. Azzarelli, J. G. Weis, S. Rochat, K. A. Mirica, J. B. Ravnsbaek and T. M. Swager, *Angew. Chem., Int. Ed.*, 2016, **55**, 1266–1281.

63 D. Tasis, N. Tagmatarchis, A. Bianco and M. Prato, *Chem. Rev.*, 2006, **106**, 1105–1136.

64 C. L. Tan, X. H. Cao, X. J. Wu, Q. Y. He, J. Yang, X. Zhang, J. Z. Chen, W. Zhao, S. K. Han, G. H. Nam, M. Sindoro and H. Zhang, *Chem. Rev.*, 2017, **117**, 6225–6331.

65 J. Kou, E. P. Nguyen, A. Merkoçi and Z. Guo, *2D Mater.*, 2020, **7**, 032001.

66 C. Mackin, A. Fasoli, M. Xue, Y. Lin, A. Adebiyi, L. Bozano and T. Palacios, *2D Mater.*, 2020, **7**, 022002.

67 T. T. Tung, M. J. Nine, M. Krebsz, T. Pasinszki, C. J. Coghlan, D. N. H. Tran and D. Losic, *Adv. Funct. Mater.*, 2017, **27**, 1702891.

68 Y. L. Guo, Y. J. Shu, A. Q. Li, B. L. Li, J. Pi, J. Y. Cai, H. H. Cai and Q. S. Gao, *J. Mater. Chem. B*, 2017, **5**, 5532–5538.

69 G. Bottari, M. Á. Herranz, L. Wibmer, M. Volland, L. Rodríguez-Pérez, D. M. Guldi, A. Hirsch, N. Martín, F. D'Souza and T. Torres, *Chem. Soc. Rev.*, 2017, **46**, 4464–4500.

70 J. Xu, Y. Wang and S. Hu, *Microchim. Acta*, 2017, **184**, 1–44.

71 C. Backes, A. M. Abdelkader, C. Alonso, A. Andrieux-Ledier, R. Arenal, J. Azpeitia, N. Balakrishnan, L. Banszerus, J. Barjon, R. Bartali, S. Bellani, C. Berger, R. Berger, M. M. Bernal Ortega, C. Bernard, P. H. Beton, A. Beyer, A. Bianco, P. Bøggild, F. Bonaccorso, G. Borin Barin, C. Botas, R. A. Bueno, D. Carriazo, A. Castellanos-Gomez, M. Christian, A. Ciesielski, T. Ciuk, M. T. Cole, J. Coleman, C. Coletti, L. Crema, H. Cun, D. Dasler, D. De Fazio, N. Díez, S. Drieschner, G. S. Duesberg, R. Fasel, X. Feng, A. Fina, S. Forti, C. Galiotis, G. Garberoglio, J. M. García, J. A. Garrido, M. Gibertini, A. Gölzhäuser, J. Gómez, T. Greber, F. Hauke, A. Hemmi, I. Hernandez-Rodriguez, A. Hirsch, S. A. Hodge, Y. Huttel, P. U. Jepsen, I. Jimenez, U. Kaiser, T. Kaplas, H. Kim, A. Kis, K. Papagelis, K. Kostarelos, A. Krajewska, K. Lee, C. Li, H. Lipsanen, A. Liscio, M. R. Lohe, A. Loiseau, L. Lombardi, M. F. López, O. Martin, C. Martín, L. Martínez, J. A. Martin-Gago, J. I. Martínez, N. Marzari, Á. Mayoral, J. McManus, M. Melucci, J. Méndez, C. Merino, P. Merino, A. P. Meyer, E. Miniussi, V. Miseikis, N. Mishra, V. Morandi, C. Munuera, R. Muñoz, H. Nolan, L. Ortolani, A. K. Ott, I. Palacio, V. Palermo, J. Parthenios, I. Pasternak, A. Patane, H. Prevost, V. Prudkovskiy, N. Pugno, T. Rojo, A. Rossi, P. Ruffieux, P. Samorì, L. Schué, E. Setijadi, T. Seyller, G. Speranza, C. Stampfer, I. Stenger, W. Strupinski, Y. Svirko, K. Taioli, K. B. K. Teo, M. Testi, F. Tomarchio, M. Tortello, E. Treossi, A. Turchanin, E. Vazquez, E. Villaro, P. R. Whelan, Z. Xia, R. Yakimova, S. Yang, G. R. Yazdi, C. Yim, D. Yoon, X. Zhang, X. Zhuang, L. Colombo, A. C. Ferrari and M. Garcia-Hernandez, *2D Mater.*, 2020, **7**, 022001.

72 E. Zor, E. Morales-Narváez, S. Alpaydin, H. Bingol, M. Ersoz and A. Merkoçi, *Biosens. Bioelectron.*, 2017, **87**, 410–416.

73 A. Kasprzak and M. Poplawska, *Chem. Commun.*, 2018, **54**, 8547–8562.

74 Y. Takagiri, T. Ikuta and K. Maehashi, *ACS Omega*, 2020, **5**, 877–881.

75 C. Göde, M. L. Yola, A. Yılmaz, N. Atar and S. Wang, *J. Colloid Interface Sci.*, 2017, **508**, 525–531.

76 H. C. Zhang and C. Li, *RSC Adv.*, 2020, **10**, 18502–18511.

77 G. Olsen, J. Ulstrup and Q. J. Chi, *ACS Appl. Mater. Interfaces*, 2016, **8**, 37–41.

78 M. Buaki-Sogo, M. del Pozo, P. Hernandez, H. Garcia and C. Quintana, *Talanta*, 2012, **101**, 135–140.

79 Y. Guo, S. Guo, J. Ren, Y. Zhai, S. Dong and E. Wang, *ACS Nano*, 2010, **4**, 4001–4010.

80 X. V. Zhen, E. G. Swanson, J. T. Nelson, Y. Zhang, Q. Su, S. J. Koester and P. Buhlmann, *ACS Appl. Nano Mater.*, 2018, **1**, 2718–2726.

81 E. Fernandes, P. D. Cabral, R. Campos, G. Machado, M. F. Cerqueira, C. Sousa, P. P. Freitas, J. Borme, D. Y. Petrovykh and P. Alpuim, *Appl. Surf. Sci.*, 2019, **480**, 709–716.

82 L. Zhou, H. Mao, C. Wu, L. Tang, Z. Wu, H. Sun, H. Zhang, H. Zhou, C. Jia, Q. Jin, X. Chen and J. Zhao, *Biosens. Bioelectron.*, 2017, **87**, 701–707.

83 G. Wu, Z. Dai, X. Tang, Z. Lin, P. K. Lo, M. Meyyappan and K. W. C. Lai, *Adv. Healthcare Mater.*, 2017, **6**, 1700736.

84 Z. Xia, F. Leonardi, M. Gobbi, Y. Liu, V. Bellani, A. Liscio, A. Kovtun, R. Li, X. Feng, E. Orgiu, P. Samorì, E. Treossi and V. Palermo, *ACS Nano*, 2016, **10**, 7125–7134.

85 B. D. Ossonon and D. Bélanger, *Carbon*, 2017, **111**, 83–93.

86 C. H. Su, H. L. Chiu, Y. C. Chen, M. Yesilmen, F. Schulz, B. Ketelsen, T. Vossmeyer and Y. C. Liao, *Langmuir*, 2019, **35**, 3256–3264.

87 Q. Fan, L. Wang, D. Xu, Y. Duo, J. Gao, L. Zhang, X. Wang, X. Chen, J. Li and H. Zhang, *Nanoscale*, 2020, **12**, 11364–11394.

88 J. Zou and J.-G. Yu, *Mater. Sci. Eng., C*, 2020, **112**, 110910.

89 F. Zhang, C. Lu, M. Wang, X. Yu, W. Wei and Z. Xia, *ACS Sens.*, 2018, **3**, 304–312.

90 P. Kassal, M. D. Steinberg and I. M. Steinberg, *Sens. Actuators, B*, 2018, **266**, 228–245.

91 N. Priyadarshni, P. Nath, Nagahanumaiah and N. Chanda, *ACS Sustainable Chem. Eng.*, 2018, **6**, 6264–6272.

92 N. Wang, Y. Liu, Y. Li, Q. Liu and M. Xie, *Sens. Actuators, B*, 2018, **255**, 78–86.

93 V. Dugandžić, S. Kupfer, M. Jahn, T. Henkel, K. Weber, D. Cialla-May and J. Popp, *Sens. Actuators, B*, 2019, **279**, 230–237.

94 L. Yang, N. Huang, L. Huang, M. Liu, H. Li, Y. Zhang and S. Yao, *Anal. Methods*, 2017, **9**, 618–624.

95 H. Yuan, W. Ji, S. Chu, Q. Liu, S. Qian, J. Guang, J. Wang, X. Han, J.-F. Masson and W. Peng, *ACS Sens.*, 2019, **4**, 704–710.

96 P. Makam, R. Shilpa, A. E. Kandjani, S. R. Periasamy, Y. M. Sabri, C. Madhu, S. K. Bhargava and T. Govindaraju, *Biosens. Bioelectron.*, 2018, **100**, 556–564.

97 A. U. Alam, M. M. R. Howlader, N.-X. Hu and M. J. Deen, *Sens. Actuators, B*, 2019, **296**, 126632.

98 V. Montes-García, R. F. de Oliveira, Y. Wang, A. Berezin, P. Fanjul-Bolado, M. B. González García, T. M. Hermans, D. Bonifazi, S. Casalini and P. Samorì, *Adv. Funct. Mater.*, 2020, 2008554.

99 W. Zhao, H. Yang, S. Xu, X. Li, W. Wei and X. Liu, *ACS Sustainable Chem. Eng.*, 2019, **7**, 17424–17431.

100 X. Chen, H. Pu, Z. Fu, X. Sui, J. Chang, J. Chen and S. Mao, *Environ. Sci.: Nano*, 2018, **5**, 1990–1999.

101 S.-J. Choi, B. Yoon, S. Lin and T. M. Swager, *ACS Appl. Mater. Interfaces*, 2020, **12**, 28375–28382.

102 H. Xu, C. Liao, Y. Liu, B.-C. Ye and B. Liu, *Anal. Chem.*, 2018, **90**, 4438–4444.

103 H. Xie, Y.-T. Li, Y.-M. Lei, Y.-L. Liu, M.-M. Xiao, C. Gao, D.-W. Pang, W.-H. Huang, Z.-Y. Zhang and G.-J. Zhang, *Anal. Chem.*, 2016, **88**, 11115–11122.

104 T. M. Godoy-Reyes, A. M. Costero, P. Gavina, R. Martinez-Manez and F. Sancenon, *ACS Appl. Nano Mater.*, 2019, **2**, 1367–1373.

105 M. I. Halawa, F. Wu, T. H. Fereja, B. Lou and G. Xu, *Sens. Actuators, B*, 2018, **254**, 1017–1024.

106 J. Budhathoki-Uprety, J. Shah, J. A. Korsen, A. E. Wayne, T. V. Galassi, J. R. Cohen, J. D. Harvey, P. V. Jena, L. V. Ramanathan, E. A. Jaimes and D. A. Heller, *Nat. Commun.*, 2019, **10**, 3605.

107 G. Bisker, N. A. Bakh, M. A. Lee, J. Ahn, M. Park, E. B. O'Connell, N. M. Iverson and M. S. Strano, *ACS Sens.*, 2018, **3**, 367–377.

108 X. Ran, Q. Qu, X. Qian, W. Xie, S. Li, L. Li and L. Yang, *Sens. Actuators, B*, 2018, **257**, 362–371.

109 A. Cao, W. Zhu, J. Shang, J. H. Klootwijk, E. J. R. Sudhölter, J. Huskens and L. C. P. M. de Smet, *Nano Lett.*, 2017, **17**, 1–7.

110 L. Qin, G. M. Zeng, C. Lai, D. L. Huang, C. Zhang, P. Xu, T. J. Hu, X. G. Liu, M. Cheng, Y. Liu, L. Hu and Y. Y. Zhou, *Sens. Actuators, B*, 2017, **243**, 946–954.

111 A. U. Alam, Y. Qin, M. Catalano, L. Wang, M. J. Kim, M. M. R. Howlader, N.-X. Hu and M. J. Deen, *ACS Appl. Mater. Interfaces*, 2018, **10**, 21411–21427.

112 G. Zhao, L. Yang, S. Wu, H. Zhao, E. Tang and C.-P. Li, *Biosens. Bioelectron.*, 2017, **91**, 863–869.

113 N. Chen, P. Ding, Y. Shi, T. Y. Jin, Y. Y. Su, H. Y. Wang and Y. He, *Anal. Chem.*, 2017, **89**, 5072–5078.

114 L. Qin, G. Zeng, C. Lai, D. Huang, C. Zhang, P. Xu, T. Hu, X. Liu, M. Cheng, Y. Liu, L. Hu and Y. Zhou, *Sens. Actuators, B*, 2017, **243**, 946–954.

115 J. Langer, D. J. de Aberasturi, J. Aizpurua, R. A. Alvarez-Puebla, B. Auguie, J. J. Baumberg, G. C. Bazan, S. E. J. Bell, A. Boisen, A. G. Brolo, J. Choo, D. Cialla-May, V. Deckert, L. Fabris, K. Faulds, F. J. G. de Abajo, R. Goodacre, D. Graham, A. J. Haes, C. L. Haynes, C. Huck, T. Itoh, M. Ka, J. Kneipp, N. A. Kotov, H. Kuang, E. C. Le Ru, H. K. Lee, J. F. Li, X. Y. Ling, S. A. Maier, T. Mayerhofer, M. Moskovits, K. Murakoshi, J. M. Nam, S. Nie, Y. Ozaki, I. Pastoriza-Santos, J. Perez-Juste, J. Popp, A. Pucci, S. Reich, B. Ren, G. C. Schatz, T. Shegai, S. Schlucker, L. L. Tay, K. G. Thomas, Z. Q. Tian, R. P. Van Duyne, T. Vo-Dinh, Y. Wang, K. A. Willets, C. Xu, H. Xu, Y. Xu, Y. S. Yamamoto, B. Zhao and L. M. Liz-Marzán, *ACS Nano*, 2020, **14**, 28–117.

116 A. J. Gillen, D. J. Siefman, S.-J. Wu, C. Bourmaud, B. Lambert and A. A. Boghossian, *J. Colloid Interface Sci.*, 2020, **565**, 55–62.

117 A. G. Beyene, A. A. Alizadehmojarad, G. Dorlhiac, N. Goh, A. M. Streets, P. Král, L. Vuković and M. P. Landry, *Nano Lett.*, 2018, **18**, 6995–7003.

118 F. A. Mann, N. Herrmann, D. Meyer and S. Kruss, *Sensors*, 2017, **17**, 1521.

119 Z. W. Li, W. S. Wang and Y. D. Yin, *Trends Chem.*, 2020, **2**, 593–608.

120 H. B. Hu, S. C. Wang, X. L. Feng, M. Pauly, G. Decher and Y. Long, *Chem. Soc. Rev.*, 2020, **49**, 509–553.

121 E. M. Hofferber, J. A. Stapleton and N. M. Iverson, *J. Electrochem. Soc.*, 2020, **167**, 037530.

122 J. Pan, F. Li and J. H. Choi, *J. Mater. Chem. B*, 2017, **5**, 6511–6522.

123 R. Peng, X. S. Tang and D. Li, *Small*, 2018, **14**, 1800013.

124 M. A. Squillaci, L. Ferlauto, Y. Zagranyarski, S. Milita, K. Müllen and P. Samorì, *Adv. Mater.*, 2015, **27**, 3170–3174.

125 S. M. Tan, A. Ambrosi, C. K. Chua and M. Pumera, *J. Mater. Chem. A*, 2014, **2**, 10668–10675.

126 A. Nag, A. Mitra and S. C. Mukhopadhyay, *Sens. Actuators, A*, 2018, **270**, 177–194.

127 W. Fu, L. Jiang, E. P. van Geest, L. M. Lima and G. F. Schneider, *Adv. Mater.*, 2017, **29**, 1603610.

128 C. Anichini, A. Aliprandi, S. M. Gali, F. Liscio, V. Morandi, A. Minoia, D. Beljonne, A. Ciesielski and P. Samorì, *ACS Appl. Mater. Interfaces*, 2020, **12**, 44017–44025.

129 G. Seo, G. Lee, M. J. Kim, S. H. Baek, M. Choi, K. B. Ku, C. S. Lee, S. Jun, D. Park, H. G. Kim, S. J. Kim, J. O. Lee, B. T. Kim, E. C. Park and S. I. Kim, *ACS Nano*, 2020, **14**, 5135–5142.

130 G. Seo, G. Lee, M. J. Kim, S.-H. Baek, M. Choi, K. B. Ku, C.-S. Lee, S. Jun, D. Park, H. G. Kim, S.-J. Kim, J.-O. Lee, B. T. Kim, E. C. Park and S. I. Kim, *ACS Nano*, 2020, **14**, 12257–12258.

131 H. Hu, A. Zavabeti, H. Quan, W. Zhu, H. Wei, D. Chen and J. Z. Ou, *Biosens. Bioelectron.*, 2019, **142**, 111573.

132 H. W. Lee, D.-H. Kang, J. H. Cho, S. Lee, D.-H. Jun and J.-H. Park, *ACS Appl. Mater. Interfaces*, 2018, **10**, 17639–17645.

133 P. Zhang, S. Yang, R. Pineda-Gómez, B. Ibarlucea, J. Ma, M. R. Lohe, T. F. Akbar, L. Baraban, G. Cuniberti and X. Feng, *Small*, 2019, **15**, 1901265.

134 S. K. Tuteja and S. Neethirajan, *Nanotechnology*, 2018, **29**, 135101.

135 C. De-Eknamkul, X. Zhang, M.-Q. Zhao, W. Huang, R. Liu, A. T. C. Johnson and E. Cubukcu, *2D Mater.*, 2019, **7**, 014004.

136 Y. Chen, R. Ren, H. Pu, J. Chang, S. Mao and J. Chen, *Biosens. Bioelectron.*, 2017, **89**, 505–510.

137 Q. Wu, N. Li, Y. Wang, Y. liu, Y. Xu, S. Wei, J. Wu, G. Jia, X. Fang, F. Chen and X. Cui, *Biosens. Bioelectron.*, 2019, **144**, 111697.

138 S. Kumar, Y. J. Lei, N. H. Alshareef, M. A. Quevedo-Lopez and K. N. Salama, *Biosens. Bioelectron.*, 2018, **121**, 243–249.

139 H. L. Chia, C. C. Mayorga-Martinez, N. Antonatos, Z. Sofer, J. J. Gonzalez-Julian, R. D. Webster and M. Pumera, *Anal. Chem.*, 2020, **92**, 2452–2459.

140 X. W. Wang, Y. H. Sun and K. Liu, *2D Mater.*, 2019, **6**, 042001.

141 M. T. Zhao, Y. Huang, Y. W. Peng, Z. Q. Huang, Q. L. Ma and H. Zhang, *Chem. Soc. Rev.*, 2018, **47**, 6267–6295.

142 N. Huang, P. Wang and D. L. Jiang, *Nat. Rev. Mater.*, 2016, **1**, 16068.

143 M. D. Allendorf, R. Dong, X. Feng, S. Kaskel, D. Matoga and V. Stavila, *Chem. Rev.*, 2020, **120**, 8581–8640.

144 M. I. G. S. Almeida, R. W. Cattrall and S. D. Kolev, *Anal. Chim. Acta*, 2017, **987**, 1–14.

145 Y. Shao, Y. Ying and J. Ping, *Chem. Soc. Rev.*, 2020, **49**, 4405–4465.

146 H. Li, Y. Zhu, M. S. Islam, M. A. Rahman, K. B. Walsh and G. Koley, *Sens. Actuators, B*, 2017, **253**, 759–765.

147 M. A. Beluomini, J. L. da Silva, A. C. de Sa, E. Buffon, T. C. Pereira and N. R. Stradiotto, *J. Electroanal. Chem.*, 2019, **840**, 343–366.

148 L. X. Chen, X. Y. Wang, W. H. Lu, X. Q. Wu and J. H. Li, *Chem. Soc. Rev.*, 2016, **45**, 2137–2211.

149 M. I. Gaviria-Arroyave, J. B. Cano and G. A. Peñuela, *Talanta Open*, 2020, **2**, 100006.

150 A. Castro-Grijalba, V. Montes-García, M. J. Cordero-Ferradás, E. Coronado, J. Pérez-Juste and I. Pastoriza-Santos, *ACS Sens.*, 2020, **5**, 693–702.

151 J. A. Hutchison, A. Liscio, T. Schwartz, A. Canaguier-Durand, C. Genet, V. Palermo, P. Samorì and T. W. Ebbesen, *Adv. Mater.*, 2013, **25**, 2481–2485.

152 D. G. Baranov, M. Wersäll, J. Cuadra, T. J. Antosiewicz and T. Shegai, *ACS Photonics*, 2018, **5**, 24–42.